ARKIV FÖR FYSIK Band 17 nr 1

Communicated 11 November 1959 by Erik Hulthén and Erik Rudberg

Precision phase contrast refractometry and its application to heavy-light water

By Erik Djurle

With 31 figures in the text

SUMMARY

The imaging of objects in the phase contrast refractometer has been treated by means of diffraction theory and the results obtained have been used in the design and construction of a new refractometer. The properties of the instrument have been examined from different aspects, e.g. the sensitivity, the demands on mechanical stability, temperature constancy etc. The measuring range is determined by the spectral properties of the lamp and monochromator and this unit has been thoroughly examined by determining the contrast at many interference periods in the instrument and also by means of a birefringent interferometer. The lower limit is set, by the photometric accuracy, to 3×10^{-8} in refractive index difference and the upper, by the monochromaticity of the spectral line, to 9×10^{-3} with a cell 30 mm long. Various experiences obtained during measurements on gases are reported. For liquids, the system heavy-light water has been thoroughly examined. The treatment of the water to give reproducible results is discussed. The refractive index difference for heavy water and ordinary water, $\Delta n = n_{D_2O} - n_{H_2O}$, has been measured at two temperatures. From these measurements, the following equations valid at 20.0°C have been obtained: $-\Delta n \times 10^7 = 48662x - 143x^2$ for $\lambda = 5461$ A and $-\Delta n \times 10^7 = 52960x - 174x^2$ for $\lambda = 4358$ A (x is the excess concentration of deuterium in the sample relative to the content in ordinary water). These equations have been compared with equations which were theoretically calculated using the Dale-Gladstone formula and the volumes of the solution and its components. The agreement shows that the refractive index of the solution is correctly described by this law. For the temperature derivative, the following values have been obtained: $\dfrac{d(\Delta n)}{dt} = +25.0x \times 10^{-6}$ for $\lambda = 5461$ A and $\dfrac{d(\Delta n)}{dt} = +26.0x \times 10^{-6}$ for $\lambda = 4358$ A. The determination of heavy water concentrations using the phase contrast refractometer gives an accuracy of 0.002 mol per cent in the low concentration region where the limit is set by the reproducibility of the treatment of the water. This corresponds to 15×10^{-8} in refractive index. For higher concentrations, the accuracy diminishes due to the errors in the equations given above and, in the highest region, it is 0.02 mol per cent. The influence of pressure on the refractive index was also examined for ordinary water and heavy water. The values obtained for the isothermal compressibility are for ordinary water 44.9×10^{-11} m^2/N and for heavy water 45.9×10^{-11} m^2/N. These values are compared with others determined by means of other methods and it is seen that the agreement is good. In this work, Dale-Gladstone's law was also used and was found to give a good description of the phenomena.

CONTENTS

Review of the development 3

I. The instrument

1. Principles of the instrument 3
2. Diffraction theory for the instrument. 4
    - 2.1. Mathematical formulae 4
    - 2.2. Vector representation of the formulae 7
        - 2.1.1. First approximation 8
        - 2.2.2. Second approximation 8
        - 2.2.3. Third approximation 9
    - 2.3. Validity of the approximate calculations for the image, and the influence of optical imperfections 10
    - 2.4. Modifications of the theory for absorbing samples 11
    - 2.5. Calculation of the intensity ratio in the image for fixed x-values. . 12
3. Description of the instrument 16
    - 3.1.1. The monochromator 17
    - 3.1.2. The refractometer part 18
    - 3.1.3. The cell and its holder 19
    - 3.1.4. The photometer 21
    - 3.1.5. The mounting of the apparatus 23
4. Adjustment and testing of the instrument. 24
5. Interferometric properties of the lamp and monochromator 26
    - 5.1. Interferometric tests 27
        - 5.1.1. Interferometric test with the refractometer 27
        - 5.1.2. Interferometric test with a birefringent interferometer 28
        - 5.1.3. Discussion of the results 29
    - 5.2. Possible displacement of the Δn-curve due to the shape of the spectral line 29
6. Measurement on gas samples 31

II. Determination of the refractive index of heavy-light water solutions

7. Experimental procedure 33
    - 7.1. Earlier investigations 33
    - 7.2. Calibration of the instrument 33
        - 7.2.1. The cell thickness 34
        - 7.2.2. The calibration curve 35
    - 7.3. The measuring technique 37
8. Precautions concerning purity of the samples 39
    - 8.1. Purification of the water 39
    - 8.2. Treatment of the distilled water 40
9. The heavy water and the measurements performed on it 43
    - 9.1. Preparation of the samples 43
    - 9.2. Changes in the D_2O in the cell. 44
    - 9.3. Measurements on the D_2O samples 45
    - 9.4. The equations for $n_{D_2O} - n_{H_2O}$ 47
    - 9.5. Comparison with earlier determinations, analytical possibilities . . . 53
10. Determination of the compressibility 54
    - 10.1. Measuring procedure 54
    - 10.2. Calculation of the compressibility 56
    - 10.3. Discussion 57

Acknowledgements 58

Review of the development

The phase contrast method, invented by Zernike, has been used in many applications, most of which have been in the field of microscopy. One of the few macroscopic arrangements is the phase contrast refractometer developed at this laboratory after the idea given by Ingelstam (1). The instrument was built so that it would give a higher precision for the measurement of refractive index differences than the existing refractometers of the Rayleigh type and also hollow prisms placed on precision spectrometers. It was also possible to make it much less sensitive to temperature influences because the thickness of the cell could be chosen shorter than was earlier required and also because the cell could be designed so that temperature equilibrium would be rapidly established.

The first laboratory arrangement (1) was changed and equipped with a better photometric unit (2). Using this instrument, a preliminary measurement on the heavy-light water system was made (3). With the experiences gained from these apparatuses, a new instrument was built for measurements on streaming gases. This work was reported in 1955 (4). The technique was further examined and also tested with liquids (5). It did not give, however, the high precision of the measurements on stationary samples. Some measurements of refractive indices in the infrared region have also been made with the phase contrast method (6). Much practical experience was gained with these instruments. However, many of the factors which influence the image formation in the instrument, e.g. the widths of the slits, focusing, the phase plate and so on, could not be examined with these arrangements since many of the details had to be given fixed dimensions. In the newly designed instrument, the influence of all these factors can be examined. In order to give the instrument suitable dimensions, it was necessary to perform a complete diffraction calculation of the image formation. The instrument has been used for measurements on stationary samples in order to get the high accuracy which is given by this case. The heavy-light water system and the influence of compression on the refractive index of the liquids have been examined.

I. THE INSTRUMENT

1. Principles of the instrument

The instrument is an one-dimensional form of the phase contrast arrangement, and it is a development of the first set-up described by Ingelstam (1). A short description of the main parts of the instrument will be given in order to make the following sections of this paper easier to follow.

A schematic view of the instrument is seen in Fig. 1. A monochromatic plane wave front is seen coming from the left. This front passes the cell in the object plane. The cell has three parts, two denoted by B and one by A. In accordance with the conditions for one-dimensional phase contrast imaging, the width of the part A is a small fraction of the whole aperture in the width direction. The gas or liquid to be examined is in part A and a reference gas or liquid in the two parts B. If the refractive index for the sample is n_1 and for the reference n_2, then the wave emerging from A will have a phase difference relative to the wave from B of

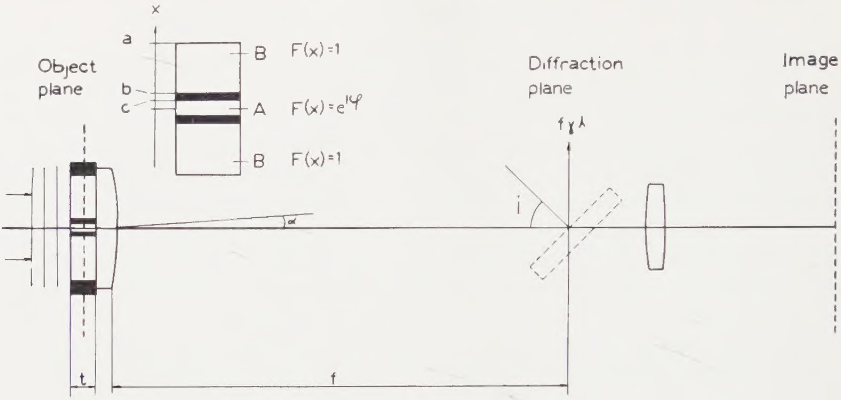

Fig. 1. The main optical parts of the phase contrast imaging system. For notations, see text.

$$\varphi = 2\pi t (n_2 - n_1) / \lambda$$

where t is the thickness of the cell.

The wave front from the cell is focused with a lens and gives, in the focal plane of this lens, the diffraction plane, a diffraction pattern which is a function of the relative phase relation and the openings in the cell. This plane is conjugate to the plane containing the entrance aperture (the plane that contains the narrow entrance slit i.e. the exit slit of the monochromator). To get the desired phase contrast imaging, the phase turning device, the phase plate, is as usual placed in this plane. It consists of an aluminised mirror with the central part in the form of a narrow step with a height which can be chosen between, for example, 700 and 3000 A. The light that is to be phase turned is focused on it. A lens placed behind the plate then gives a phase contrast image of the cell in the image plane. The intensity ratios in the image are measured by means of a special photometer. The phase differences in the light amplitudes from the cell, and the corresponding refractive index differences are then calculated. Only samples with negligible absorption give measurements of high accuracy.

2. Diffraction theory for the instrument

2.1 *Mathematical formulae*

The imaging of objects with phase contrast has been treated for one- and two-dimensional cases by several authors using diffraction theory. Bennet *et al.* (7) have made calculations for the two-dimensional case, in particular for microscopes. The calculations by Schmidt (8) and by Wolter (9, 10) are more general and although they were made for one-dimensional microscope cases they can be applied, in part, to the phase contrast refractometer. (In the Encyclopedia of Physics (10), Wolter has given a reference list containing the main works in the field up to 1956.)

The following notations will be used:

a, b, c = height coordinates in the object plane
b–c = thickness of the opaque wall between the A- and B-parts of the cell.

f = focal length of the lens which refracts the plane wave front to its diffraction plane

α = the diffraction angle from the aperture

γ = $\sin\alpha / \lambda$, normalized angular measure of the diffraction angle (since α is small $\sin \alpha = \alpha$). γ is also the angular coordinate in the diffraction plane, i.e. the normalized linear coordinate divided by the focal length f.

$\varkappa$ = decentering measure of the image position of the entrance slit on the phase step.

ψ = phase advance produced by the central zone of the phase plate—for the completely metal-coated mirrors used here, it is

$$\psi = \frac{4\pi z \cos i}{\lambda}$$

z = height of the step on the phase plate

i = incidence angle

In order to make the calculations less complicated, some simplifying assumptions will be made: The wave front passing the object is plane and ideal, i.e. all the lenses and the grating in the monochromator are free from aberrations and there are no apertures which introduce diffraction phenomena that modify the wave front. The only apertures are at the cell and at the phase plate. The entrance slit is infinitely narrow and the lens in front of the object ideal. The lens that gives the phase contrast image is also assumed ideal. The magnification in this imaging is chosen to be unity.

The wave front leaving the cell has only one-dimensional variations. Its amplitude can be written $F(x) = \exp i\varphi$ because there is no absorption. φ is the phase angle and is zero for the B-parts i.e. $F(x) = 1$ for these areas. This wave undergoes diffraction as it passes through the openings in the cell. The amplitude $G(\gamma)$ in the diffraction plane of the diffracted wave corresponding to an angle α with the optical axis (Fig. 1) is equal to the Fourier transform (9, 11) of $F(x)$, i.e. $F(x)$ is multiplied by $\exp(-i2\pi x\gamma)$ and integrated over the aperture 0.

$$G(\gamma) = \int_{0} F(x)\, e^{-i2\pi x\gamma} dx$$

With $F(x)$ as above and with symmetrical limits for the integral, we thus get, for an infinitely narrow entrance slit, the following amplitudes in the diffraction plane

$$G(\gamma) = 2a\frac{\sin 2\pi a\gamma}{2\pi a\gamma} - 2b\frac{\sin 2\pi b\gamma}{2\pi b\gamma} + 2c\,e^{i\varphi}\frac{\sin 2\pi c\gamma}{2\pi c\gamma} \qquad [1]$$

The first term corresponds to the diffraction pattern of the whole opening without the bars (cf. Fig. 1). The second term is negative and corresponds to the bars and the central area. For mathematical convenience, light amplitudes with the same phase as for the outer openings and coming from the bars and the central area were added to the first integral to give it a simple shape. Thus, the second term compensates for the whole area between $-b$ and $+b$, and the last term, which includes the phase φ, is for the light from the central area.

The next mathematical step, which gives the image of the cell in the image plane (Fig. 1), corresponds to an inverse Fourier transform of the light amplitudes that leave the diffraction plane. They must, however, first be multiplied by a function $Q(\gamma)$ that is determined by the reflection (or transmission) properties of the phase plate. Since the plate has the same reflection coefficient over its whole surface, the reflectivity can be put equal to unity. With the angular coordinates $\pm\gamma_0$ corresponding to the boundaries of the phase plate and $2\gamma_1$ corresponding to the width of the phase turning strip, we get $Q(\gamma)=0$ for $|\gamma|>\gamma_0$, $Q(\gamma)=1$ for $\gamma_1<|\gamma|<\gamma_0$ and $Q(\gamma)=\exp i\psi$ for $|\gamma|<\gamma_1$. Since the object is symmetrical and since unit magnification has been assumed, we can use the same coordinate x in the image as in the object.

The light amplitudes in the image are thus

$$F'(x)=\int\limits_{\text{phase plate}} Q(\gamma)\,G(\gamma)\,e^{i2\pi x\gamma}d\gamma \qquad [2]$$

$F'(x)$ is here valid for a narrow slit. In order to compare the theoretical image intensities $F'F'^*$ with those experimentally measured, it is necessary to make another integration over the finite width of the entrance slit. This corresponds to summing the intensities in overlapping, noncoherent phase contrast images. It is only the image corresponding to the middle of the entrance slit which has its diffraction pattern cut in a symmetrical way by the step of the phase plate and the boundaries. The two limits for the integral [2] are thus not symmetrical, a small amount $\varkappa$ must be added to them. For large arguments, the sine and cosine integrals have small oscillating differences from a constant value. The change in the integral caused by $\varkappa$ corresponds here to only a small fraction of the period of oscillation. The outer limits of the phase plate can as a first approximation be put equal to a constant, $\pm\gamma_0$, (cf. below where $\gamma_0\to\infty$) while the limits for the phase strip are $-\gamma_1+\varkappa$, $\gamma_1+\varkappa$. Taking into account the properties of the sine and cosine integrals, we get after some calculations

$$F'(x)=F_0'(x)+(e^{i\psi}-1)\frac{1}{2\pi}\left[f_{\mathrm{Si}}(x)+i\,g_{\mathrm{Ci}}(x)+e^{i\varphi}\{h_{\mathrm{Si}}(x)+i\,k_{\mathrm{Ci}}(x)\}\right] \qquad [3]$$

$F_0'(x)$ is the image obtained without phase contrast, i.e.

$$\begin{aligned} F_0'(x)=\frac{1}{\pi}[&\mathrm{Si}\,2\pi\gamma_0(a+x)+\mathrm{Si}\,2\pi\gamma_0(a-x)-\mathrm{Si}\,2\pi\gamma_0(x+b)+\\ &+\mathrm{Si}\,2\pi\gamma_0(x-b)+e^{i\varphi}\{\mathrm{Si}\,2\pi\gamma_0(x+c)-\mathrm{Si}\,2\pi\gamma_0(x-c)\}] \qquad [4]\end{aligned}$$

f, g, h and k are the following functions

$$\begin{aligned}
f_{\mathrm{Si}}(x)=&\ \mathrm{Si}\,2\pi(\gamma_1+\varkappa)(a+x)+\mathrm{Si}\,2\pi(\gamma_1+\varkappa)(a-x)+\mathrm{Si}\,2\pi(\gamma_1-\varkappa)(a+x)+\\
&+\mathrm{Si}\,2\pi(\gamma_1-\varkappa)(a-x)-\mathrm{Si}\,2\pi(\gamma_1+\varkappa)(x+b)+\mathrm{Si}\,2\pi(\gamma_1+\varkappa)(x-b)-\\
&-\mathrm{Si}\,2\pi(\gamma_1-\varkappa)(x+b)+\mathrm{Si}\,2\pi(\gamma_1-\varkappa)(x-b)\\
g_{\mathrm{Ci}}(x)=&\ \mathrm{Ci}\,2\pi(\gamma_1+\varkappa)(a-x)-\mathrm{Ci}\,2\pi(\gamma_1+\varkappa)(a+x)-\mathrm{Ci}\,2\pi(\gamma_1-\varkappa)(a-x)+\\
&+\mathrm{Ci}\,2\pi(\gamma_1-\varkappa)(a+x)-\mathrm{Ci}\,2\pi(\gamma_1+\varkappa)(x-b)+\mathrm{Ci}\,2\pi(\gamma_1+\varkappa)(x+b)+\\
&+\mathrm{Ci}\,2\pi(\gamma_1-\varkappa)(x-b)-\mathrm{Ci}\,2\pi(\gamma_1-\varkappa)(x+b)\\
h_{\mathrm{Si}}(x)=&\ \mathrm{Si}\,2\pi(\gamma_1+\varkappa)(x+c)-\mathrm{Si}\,2\pi(\gamma_1+\varkappa)(x-c)+\mathrm{Si}\,2\pi(\gamma_1-\varkappa)(x+c)-\\
&-\mathrm{Si}\,2\pi(\gamma_1-\varkappa)(x-c)\\
k_{\mathrm{Ci}}(x)=&\ \mathrm{Ci}\,2\pi(\gamma_1+\varkappa)(x-c)-\mathrm{Ci}\,2\pi(\gamma_1+\varkappa)(x+c)-\mathrm{Ci}\,2\pi(\gamma_1-\varkappa)(x-c)+\\
&+\mathrm{Ci}\,2\pi(\gamma_1-\varkappa)(x+c)
\end{aligned}$$

If x is changed to $-x$ in [3] we get

$$F'(-x) = F_0'(x) + (e^{i\varphi} - 1)\frac{1}{2\pi}\left[f_{\mathrm{Si}}(x) - i\,g_{\mathrm{Ci}}(x) + e^{i\varphi}\{h_{\mathrm{Si}}(x) - i\,k_{\mathrm{Ci}}(x)\}\right] \qquad [5]$$

because of the properties of F_0', f, g, h and k. In the calculations which follow, these functions are calculated for positive x-values and $F'(-x)$ is obtained from [5]. A change of $\varkappa$ to $-\varkappa$ in f, g, h and k causes a change in sign for g and k. At a point x with a positive $\varkappa$-value, i.e. when the phase plate is moved in a positive direction relative to the point of symmetry in the diffraction pattern, the light amplitude is the same as that for a point $-x$ with a negative $\varkappa$ of the same magnitude. This also follows at once from the physical point of view since the optical arrangement is assumed symmetrical. It is thus only necessary to calculate the f, g, h and k functions for positive x and $\varkappa$ values. The light amplitudes are then obtained as follows

x pos. $\varkappa$ pos. insert the values in equ. [3].
x neg. $\varkappa$ neg. insert the values in equ. [3].
x pos. $\varkappa$ neg. insert the values in equ. [5].
x neg. $\varkappa$ pos. insert the values in equ. [5].

In the calculation of $F_0'(x)$ by means of formula [4], the approximation of putting the limits equal to constant values independent of $\varkappa$ means that the cosine integral terms are neglected. These cosine terms would have appeared in the same way as in the g and k functions and would thus have cancelled each other apart from small differences that have only a very small influence on the image. In evaluating formula [4], the limit γ_0 can, as another approximation, be extended to infinity. With the chosen dimensions for the cell and the particular phase plate in the instrument, the arguments of the sine integrals vary from eighty to some thousands. In this interval, the value of the integral oscillates around the value $\pi/2$ (the value for infinite argument) with an amplitude of 0.01. This small variation can be neglected because the maximum error is less than 1 %. We thus get $F_0'(x) = 1$ for $b < |x| < a$ and $F_0'(x) = e^{i\varphi}$ for $|x| < c$.

2.2 *Vector representation of the formulae*

A calculation of the intensity (the square of $|F'|$) for the image field using formulae [3], [4] and [5] for various φ-values is rather tedious. It is better to transfer them to vector diagrams (1, 12)—the intensities are then obtained as the square of the resultant vectors.

In order to make the vector diagrams less complicated, the formulae must be more or less simplified. In all approximations, $\varkappa$ is set to zero and the limits γ_0 to infinity which implies that the light amplitudes diffracted outside the phase plate are neglected. In addition, no integration corresponding to the width of the entrance slit is performed. Asymmetry effects are thus neglected and the diffraction pattern therefore corresponds to an infinitely narrow entrance slit. Putting $x = 0$ in formula [3], we get for the light amplitudes for the central area of the image (γ_0 shall later be extended to ∞)

$$F'(0)\frac{\pi}{2} = \mathrm{Si}\,2\pi a\gamma_0 - \mathrm{Si}\,2\pi a\gamma_1 + e^{i\psi}\,\mathrm{Si}\,2\pi a\gamma_1 - (\mathrm{Si}\,2\pi b\gamma_0 - \mathrm{Si}\,2\pi c\gamma_0) + \\ + (1-e^{i\psi})(\mathrm{Si}\,2\pi b\gamma_1 - \mathrm{Si}\,2\pi c\gamma_1) + (e^{i\varphi}-1)(\mathrm{Si}\,2\pi c\gamma_0 - \mathrm{Si}\,2\pi c\gamma_1) + \\ + e^{i\psi}(e^{i\varphi}-1)\,\mathrm{Si}\,2\pi c\gamma_1 \qquad [6]$$

2.2.1 *First approximation*

The first approximation is made as follows:

The influence of the bars are neglected, i.e. the terms $\mathrm{Si}\,2\pi b\gamma_i - \mathrm{Si}\,2\pi c\gamma_i = 0$ $(i = 0, 1)$. All direct light falls within the phase strip and is thus phase turned through an angle ψ, i.e. $\mathrm{Si}\,2\pi a\gamma_1 = \pi/2$. The diffracted light falling on the phase strip is neglected, i.e. $\mathrm{Si}\,2\pi c\gamma_1 = 0$ and, in addition, $\gamma_0 = \infty$. We thus get $F'(0) = e^{i\psi} + (e^{i\varphi} - 1)$.

This gives the image vector diagram shown in Fig. 2. The vector OB corresponds to the light amplitude with a phase angle φ coming from the central area of the object. This vector can be obtained by combining the vectors OA and AB. The vector OA is turned through an angle ψ and, in order to make the summation of the vectors easier when φ varies, it is placed in the position $O'A$. It corresponds to the first term and thus to the light amplitudes falling within the phase strip. The vector AB is equal to $e^{i\varphi} - 1$ and thus varies with φ. The light amplitude is the sum $O'A + AB = O'B$. For every period of φ, the intensity in the image has therefore a sinusoidal variation and goes through a minimum and a maximum with the relative intensities $(O'B')^2$ and $(O'B'')^2$ respectively (cf. section 3. Fig. 15). The maximum achievable contrast is a function of these intensities. To get a high contrast, the point O' should lie near the periphery of the circle, i.e. the step of the phase plate should have a suitable height. This simple vector diagram is often used to give a rough estimation of the properties of the phase plate. (Since it is difficult to examine the height and the width of the step with a greater precision than what corresponds to calculations using this approximation theory, it is not necessary to calculate the height of the step of the phase plate more exactly.)

2.2.2 *Second approximation*

The same simplifications as in the preceding approximation are made except that the diffracted light amplitudes falling on the phase strip are not now neglected but considered to be phase turned, i.e. $\mathrm{Si}\,2\pi c\gamma_1 \neq 0$.

Formula [6] now gives, letting $\gamma_0 \to \infty$:

$$F'(0) = e^{i\psi}\left[1 + (e^{i\varphi}-1)\frac{2}{\pi}\,\mathrm{Si}\,2\pi c\gamma_1\right] + (e^{i\varphi}-1)\left(1 - \frac{2}{\pi}\,\mathrm{Si}\,2\pi c\gamma_1\right)$$

Comparing with the previous vector diagram, we see that to the phase turned vector has been added that fraction, viz. $(2/\pi)\,\mathrm{Si}\,2\pi c\gamma_1$, of the vector $(e^{i\varphi} - 1)$, i.e. of the vector AB, which corresponds to the light amplitudes falling on the phase strip. We get the diagram in Fig. 3. The vector $OC = OA + AC$ is turned through the angle ψ. The intensity in the image is obtained as before by squaring the vector $O'B = O'C + CB$. However, as φ varies, the vector AB changes and thus also the part of it that is added to OA. The point C will move on a circle with its center situated somewhere along the OA direction and thus the point O' will move in a similar circle. The ratio

$AC/CB = (2/\pi)\,\mathrm{Si}\,2\pi c\gamma_1/[1-(2/\pi)\,\mathrm{Si}\,2\pi c\gamma_1]$ can, as $\mathrm{Si}\,u \simeq u$ for small arguments, be written $AC/CB = 4c\gamma_1$. (With the dimensions chosen, this corresponds to about a tenth of the vector since the argument in the sine integral is about 0.15.) The radius of the circle passing through A and C is thus $2c\gamma_1$. The centre of the circle for O' is a point given by the vector from O to the centre of the circle for A turned through an angle ψ. The equation for this circle in polar coordinates referred to its centre is $r = 4c\gamma_1 \sin(\psi/2)\,\exp i(\varphi+\psi/2-\pi/2)$. (A comparison with the result obtained by Ingelstam, Ref. (1) part 2.2, indicates a disagreement. It is probable that Ingelstam has made some mistake when approximating and thus arrived at an incorrect result.) The contrast that this vector diagram gives is, for the same ψ-value, lower than that obtained with the first approximation theory. The sine shape is, however, the same.

2.2.3 *Third approximation*

The only approximations made in this case are that the light amplitudes outside the phase plate can be neglected, the entrance slit is infinitely narrow and the strip of the phase plate is situated symmetrically to the diffraction pattern. As in the previous approximations, the influence of the bars is also neglected here. We get

$$F'(0) = 1-\frac{2}{\pi}\,\mathrm{Si}\,2\pi a\gamma_1 + e^{i\psi}\left[\frac{2}{\pi}\,\mathrm{Si}\,2\pi a\gamma_1 + (e^{i\varphi}-1)\frac{2}{\pi}\,\mathrm{Si}\,2\pi c\gamma_1\right] + $$
$$+(e^{i\varphi}-1)\left(1-\frac{2}{\pi}\,\mathrm{Si}\,2\pi c\gamma_1\right)$$

which gives the vector diagram Fig. 4. Comparing with the previous case, we see that the phase turned part of the direct light is now $(2/\pi)\mathrm{Si}2\pi a\gamma_1$ which can be larger than unity due to the properties of the sine integral. The direct light falling within the phase strip corresponds to the vector OA'. To OA' is added as before that part of AB which is phase turned, i.e. $AC = A'C'$. The vector that is turned is thus OC'. The correction to the previous approximation is the vector $AA' = CC' = 1-(2/\pi)\,\mathrm{Si}\,2\pi a\gamma_1$ which corresponds to the direct light falling outside the phase strip. The light amplitude for different φ-values is as before $O'B = O'C' + C'C + CB$. When φ varies, the point C moves in a circle and the point C' in another circle with the same radius but displaced through the distance AA'. The same is valid for the circle describing the movement of O'.

The diagrams in Figs. 2, 3 and 4 are all valid for $x=0$. For $x \neq 0$, formula [3] gives, according to the first approximation theory, $F'(x) = e^{i\psi}$, i.e. the light amplitude and thus the intensity, $I = e^{i\psi}e^{-i\psi} = 1$, are constant and independent of φ and x for the reference areas of the object. The light amplitude vector is $O'A$ in Fig. 2.

In the second approximation, the reference light amplitudes, i.e. $x \neq 0$, can be expected to correspond to the vector $O'A$ in Fig. 3. However, formula [3] shows that the part AC of the vector AB is a function of x, so each diagram is only valid for a fixed x-value. The point O' in these diagrams changes its position in the same way as in Fig. 3 and gives a small sinusoidal variation in the intensity $(O'A)^2$ as φ varies. The variation of the intensity with x is symmetrical and changes slowly.

The third approximation shows that both AC and AA' in Fig. 4 are functions of x and the diagrams in this case are even more complicated.

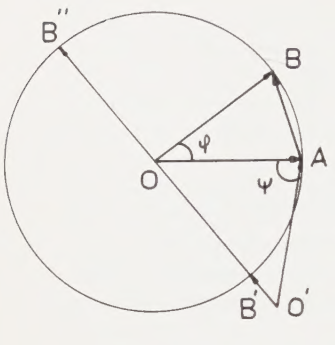

Fig. 2.

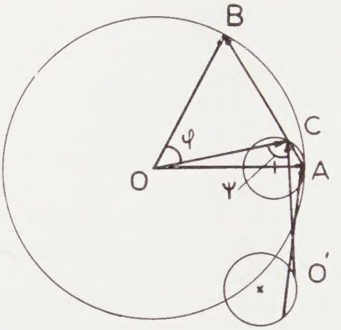

Fig. 3.

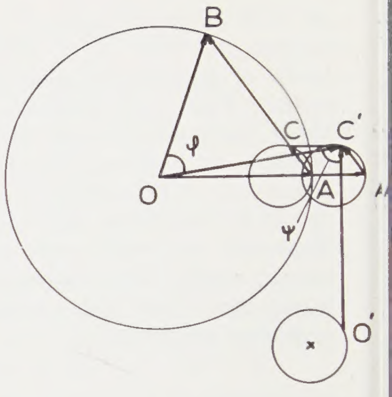

Fig. 4.

Fig. 2. Vector diagram of the phase contrast imaging, first approximation theory.

Fig. 3. Vector diagram for the second approximation theory.

Fig. 4. Vector diagram showing the correction for direct AA' and diffracted light AC falling outside and within the phase strip of the phase plate.

In all approximations above, the influence of the bars has been neglected. The correction from them appears as a correction to the vector OA in the diagrams in the same way as in Fig. 4. The intensity of these bars corresponds to the vector OO' in the simple diagram Fig. 2.

The treatment of the intensities in the phase contrast image by means of vector diagrams becomes rather complicated as soon as more terms are used in the theory for the imaging than in the first approximation. The vector diagram in Fig. 2 can be used to give a schematic view of the intensities in an image but it is not possible to use it to calculate φ-values, as have been done in some cases (13), from measured intensities because the correction terms from the diagrams in Figs. 3 and 4 must be incorporated. Even in these diagrams, certain corrections are neglected—they are, however, of a smaller influence. (With the actual c and γ_1-values used, the diagrams in Figs. 2 and 3 both give for $\psi = \pi/2$ the same minimum intensities but more than a 20 % difference in the maximum intensities.)

2.3 *Validity of the approximate calculations for the image, and the influence of optical imperfections*

The finite width of the phase plate ($\gamma_0 \neq \infty$) gives rise to the well-known diffraction fringes at boundaries in the image. The fringes have low intensity variations and, by giving the phase plate and the imaging system following it apertures of a suitable size, this effect can be made negligibly small (Fig. 5*a*).

The effect of the finite width of the phase strip is obtained from the second and third approximations. The phase turned part of the diffracted light gives a small intensity variation while the part of the direct light falling outside the strip gives large boundary effects of the same kind as those obtained when the imaging aperture is limited to $2\gamma_1$, i.e. all borders are rather diffuse and light is diffracted outside the

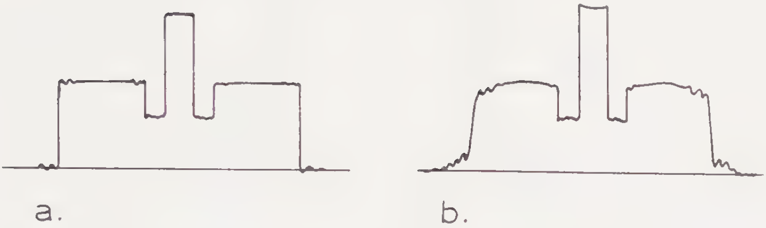

Fig. 5. Intensity distribution in the image. a. The ideal distribution modified by the outer boundaries of the phase plate. b. Modified by the diffraction by the step of the phase plate.

geometrical image, compare calculations by Wolter (9). The image intensity is as shown in Fig. 5*b* and, also, in Fig. 15 in Ref. (1) which contains photometrically scanned intensity curves of the phase contrast image for different q-values.

The influence of the optical imperfections on the image is difficult to calculate. The entrance slit must have a certain width if the intensity is not to be too small to permit measurements. Equation [3], which is calculated for an infinitely narrow slit, must be integrated over the slit width if the light from it is coherent, otherwise the square of $F'(x)$ must be integrated over it. Since the entrance slit is the exit slit of a monochromator with an optical system, the light from it is partially coherent so the integration will be a mixture of the two cases. Spherical aberrations in the lenses make the assumed plane wave front curved and local imperfections put humps in it. Imperfections in the monochromator give a non-uniform illumination in the solid angle at its exit slit. The light amplitude in the assumed plane wave front is thus not constant, so all diffraction patterns have to be modified.

The conclusion must be that, for precision measurements with phase contrast, it is not practical to calculate the exact relation between the phase difference q in the object and the contrast in the image due to the fact that there are many factors, difficult to control, which influence it. Moreover, if the windows of the cell are curved or not parallel, then the position of the diffraction pattern on the phase plate will be altered when the refractive index for the reference substance is changed. A readjustment of the pattern can give a small change in the q-intensity relation. It is thus necessary to determine the calibration curve for q in such a way that it is measured under as nearly as possible the same conditions as for the samples.

2.4 *Modifications of the theory for absorbing samples*

The calculations in the preceding sections and the vector diagrams describing them have to be modified if there is an absorption of the light in the cell. Two cases can occur, viz. the absorption in the sample and reference parts can be either equal or different for the wave length used. In the first case, the light amplitudes are all reduced by the same factor and the calculations therefore remain valid. The second case gives a combined phase and amplitude contrast imaging. The result will be that the vectors OB in the diagrams, Fig. 2–4, are shorter or longer. It is, in principle, possible to calculate the phase from these diagrams and from the modified formulae when the amplitudes are known. The amplitude can be measured in the instrument without phase contrast imaging. This can be achieved, for example, by inserting a

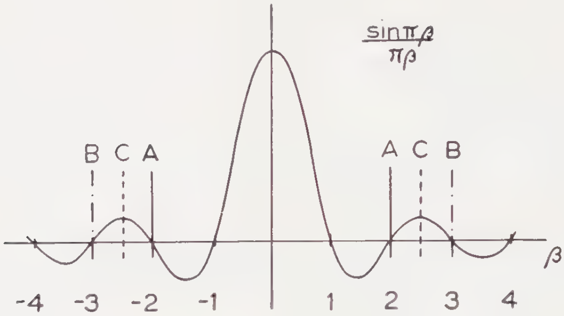

Fig. 6. The diffraction pattern from the whole aperture. β is in diffraction units. A, B and C correspond to the widths of the different phase steps in the calculations.

glass wedge in the light beam near the cell. The image on the phase plate will then be shifted outside the step and an ordinary image of the object will be obtained. However this procedure for evaluating q cannot give the highest accuracy. In order to get it, it is necessary to restrict the measurements to samples that have the same absorption for the wave length region used or an absorption difference which, at most, corresponds to the maximum error in the matching of the two light beams in the photometer. For the author's instrument, this corresponds to 0.5 % in intensity. No errors due to absorption influenced this investigation because the reference and sample substances were both pure water.

2.5 *Calculation of the intensity ratio in the image for fixed x-values*

In the photometric measurements, the intensity ratio (A/B) for the central area relative to an area in the reference field is measured (2) in order to cancel intensity fluctuations in the lamp. Although formulae [3]–[5] cannot be used to calculate a calibration curve for the instrument, it is of value, for the dimensioning of the instrument, to calculate how this ratio depends on the width of the entrance slit and the step of the phase plate. With a little extra work, a calculation of the largest allowable influence of an asymmetrical adjustment of the phase plate can be obtained. This gives an indication of what degree of mechanical stability is necessary for the instrument.

Formulae [3]-[5] are valid for an infinitely narrow entrance slit illuminated with monochromatic light. An integration of them corresponding to the width of the spectral line was not performed since the influence on the intensities in the image from this integration is at most of the same order as the influences due to the other approximations made. The calculations below are made with the following assumptions:

a. The x-values are zero and $a/2$. The coordinates a, b and c are in the ratio 45:3:1. This gives simple arguments in the formulae and, in addition, roughly corresponds to the actual dimensions of the cell and to the actual positions of the photometer slits in the image of the cell.
b. The step of the phase plate corresponds to an angle $\psi = \pi/2$.

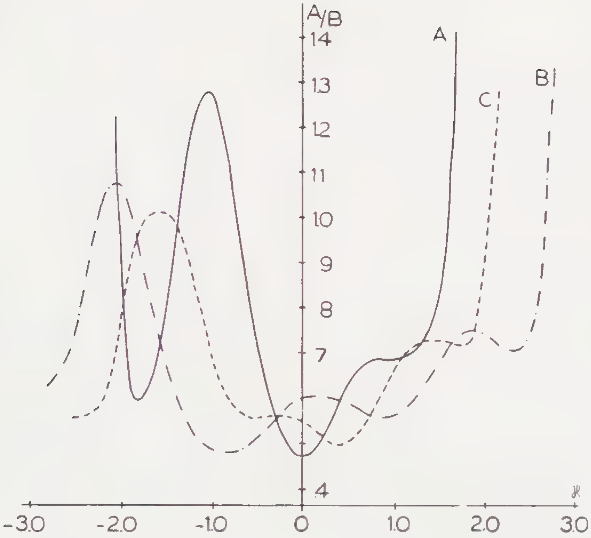

Fig. 7. The intensity ratio for a narrow entrance slit and asymmetrical measurement in the image as a function of the decentering of the image position of the entrance slit on the phase plate. $\varkappa$ is in diffraction units. The letters A, B and C correspond to the different widths of the step of the phase plates, cf. Fig. 6.

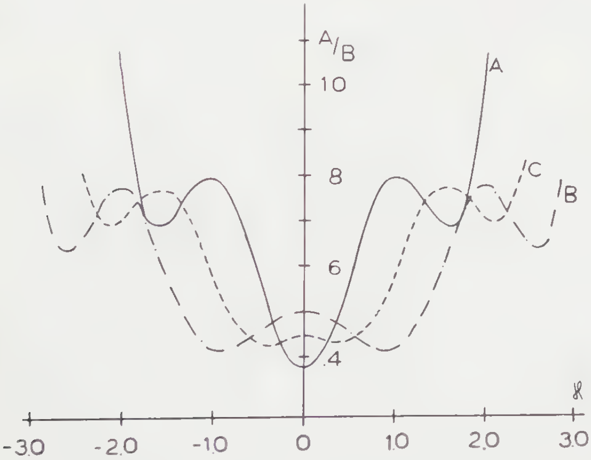

Fig. 8. The same relation as in Fig. 7 but with symmetrical measurement in the image plane.

c. The phase angle $\varphi = 0$. (It is chosen so as to make it easier to compare measured and calculated curves.)
d. The exit slit of the monochromator is an incoherent light source.
e. The optical system is perfect and the focusing thus without errors.

In the calculations, three different widths have been used for the step of the phase plate. They correspond to an intersection of the main diffraction pattern at ± 2,

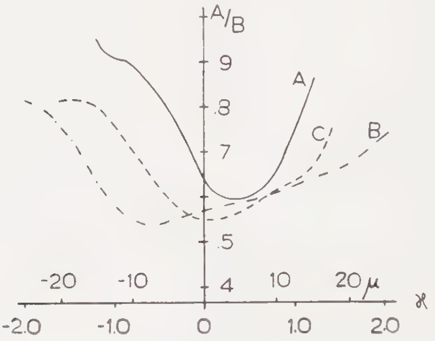

Fig. 9.

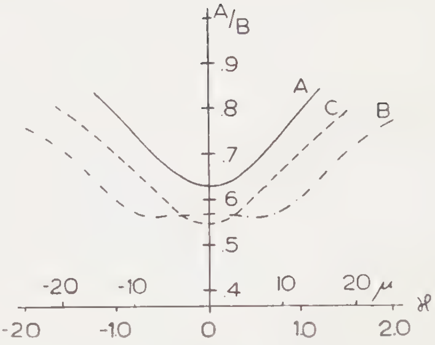

Fig. 10.

Fig. 9. Intensity ratio for asymmetrical measurement as a function of the decentering. The entrance slit is 20 μ wide. The letters A, B and C correspond to the different widths of the step of the phase plates, cf. Fig. 6.

Fig. 10. The same relation as in Fig. 9 for the photometer slits placed symmetrically in the image.

±2.5 and ±3 diffraction units (Fig. 6) i.e. the width of the step corresponds to 4, 5 or 6 units. The diffraction unit corresponds to the distance between the minima in the intensity diffraction pattern of a thin slit imaged by the whole aperture. Previous experience has indicated that a narrow step of the order of 2–3 units requires a very stable experimental arrangement while broad steps give low contrast, cf. the vector diagram for the second approximation, and are thus unsuitable. The interval for the decentering $\varkappa$ has been chosen to be 0.2 units.

The curves in Fig. 7 and 8 show the intensity ratio as a function of $\varkappa$ for the two cases when the ratio is measured with reference light from only one or from both reference fields and the entrance slit is infinitely narrow. The curves for symmetrical measurements are preferable because they have a broader minimum than the asymmetrical ones. They also show that wider phase steps are better than narrow ones, cf. A and B in the figures, from the point of view of adjustment and influence of small changes in $\varkappa$. To get the variation in the actual case, these curves have to be integrated over a $\varkappa$-interval corresponding to the width of the entrance slit. As a first approximation, the slit can be chosen a little smaller than the width of the main lobe in the diffraction pattern, i.e. 20 μ. One diffraction unit corresponds to 12.5 μ if the whole aperture is free from optical defects. The pattern will, however, be broader in the actual case. The result of the graphical integration of the curves in Figs. 7 and 8 for this slit width is shown in Fig. 9 for the unsymmetrical photometric measurement and in Fig. 10 for the symmetrical one, $\varkappa$ being expressed in diffraction units and length in μ along the normal to the optical axis at the phase step. It is obvious from the figures that the symmetrical measurement case is preferable and only this one will therefore be further discussed. An unsymmetrically measuring photometer has been used earlier (2) but proved unsatisfactory. The photometer used for this investigation was therefore constructed so that is measures symmetrically. The minima for the curves in Fig. 10 are broader, the wider the step on the phase plate. This means that the instrument is not so sensitive to a misalignment when a wider step is used. The tolerance in intensity ratio variation for precision measurements with the instrument is about 0.5 %—this corresponds to the sensitivity of the photometer. These cir-

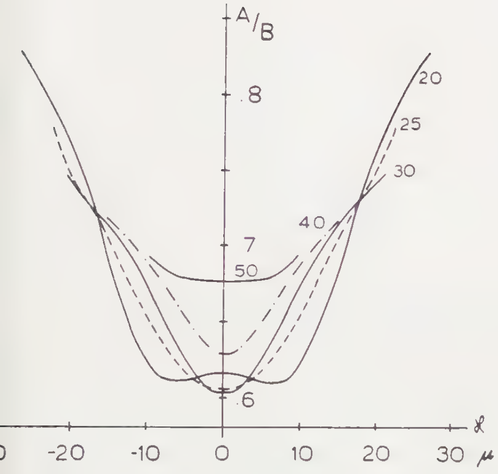

Fig. 11.

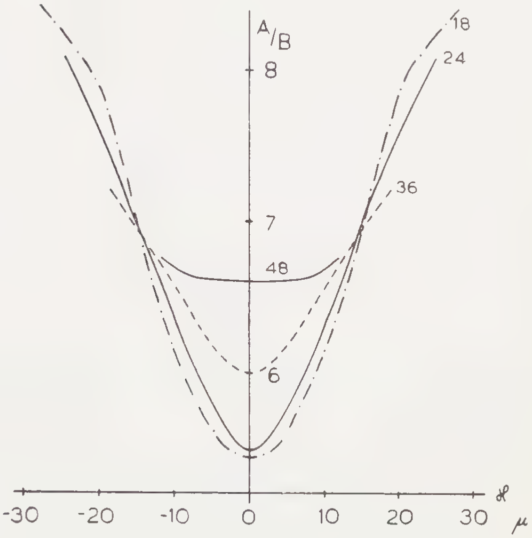

Fig. 12.

Fig. 11. The intensity ratio in the image plane as a function of the decentering of the image position of the entrance slit on the phase step for different wide entrance slits. The width of the step corresponds to case B, Fig. 6. The slit widths are in microns and are given at the respective curves.
Fig. 12. The same relations as in Fig. 11. The width of the phase step corresponds to case C, Fig. 6.

cumstances indicate that the step should be chosen as wide as possible but, as mentioned above, the variation of the contrast with φ diminishes when the step becomes broader. As a compromise, the width of the phase step is chosen to be 5–6 diffraction units. Such a width gives a good contrast and reasonable demands on mechanical stability (cf. below). The curve for a width of 4 units (Fig. 10) shows an allowable variation of a few μ while the curve for 6 units permits about $\pm 8\ \mu$.

The calculations above are valid for a fixed entrance slit and different phase plates. It is, however, also important to choose a suitably wide entrance slit since the amount of light in the instrument is of fundamental importance for the accuracy with which the two light beams in the photometer can be matched. Because it is not certain that the width of the manufactured phase step corresponds exactly to 5 or 6 units but rather to a value between them, the influence on the intensity ratio of the width of the entrance slit has been calculated for these two cases, Figs. 11 and 12. (The ordinate scale is different to that in the preceding figures.) Both figures show that a very narrow slit gives a broad minimum (cf. also corresponding curve in Fig. 8). As the slit width increases, the minimum becomes at first less pronounced but then grows wider again when the geometrical dimension of the slit image begins to fill the width of the phase step.

The calculated curves have to be compared with measured ones. The instrument is equipped with three different phase plates to make it as versatile as possible, cf. below. This means that the curves, like Fig. 12, for all phase plates have to be compared with each other. The curves also change in appearance with the phase difference

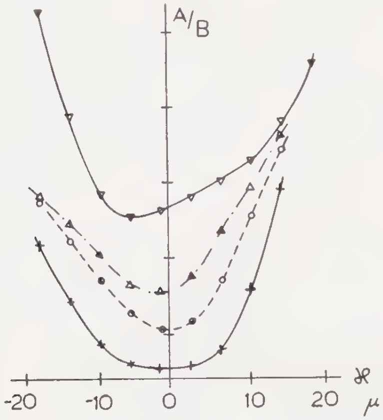

Fig. 13.

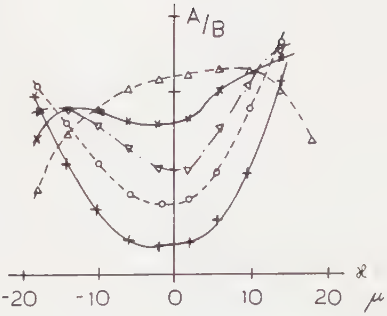

Fig. 14.

Fig. 13. Measured intensity ratio as a function of the decentering of the diffraction pattern on the phase plate for different wide entrance slits. $\varphi = 0$. One scale division on the A/B-axis corresponds to 0.25 mm in the drum reading, i.e. an intensity ratio increase of about 7 %, the intensity scale being logarithmic. The following widths for the entrance slit were used: 20 μ − + − + − + −, 30 μ − ○ − ○ −, 38 μ − △ − △ − and 54 μ − ▽ − ▽ −.

Fig. 14. The same relations as in Fig. 13 with $\pi = \varphi/2$. The widths for the entrance slit were: 20 μ − + − + − + −, 30 μ − ○ − ○ − ○ −, 38 μ − ▽ − ▽ −, 46 μ − × − × − and 54 μ − △ − △ −.

φ. Figs. 13 and 14 show measurements at best focus for a plate with $\psi \eqsim 80^\circ$ at $\varphi = 0$ and $\varphi \eqsim \pi/2$. As for the theoretical curves, a narrow slit gives a broad minimum for different φ-values while a wide slit, e.g. the curve for 54 μ, can give a broad maximum or minimum depending on the φ-value. All curves are asymmetrical—this must be due to asymmetry in the optical system. This effect is more marked for the outer two phase plates that are placed on either side of the plate with $\psi \simeq 80^\circ$ which is on the optical axis. All curves, theoretical and measured, thus indicate that the entrance slit ought to be very narrow or of the order of 50 μ. A study of the curves for all three phase plates shows that it is better to choose a narrow slit rather than a wide one because the curves then have a better appearance. A slit of 25 μ width was therefore chosen — it gives, in addition, sufficient light in the image for the desired photometric sensitivity.

3. Description of the instrument

The change in the intensity ratio as a function of the phase difference is sinusoidal, as shown in section 2. It is the steep parts of this curve that are used for precision measurements. It is thus necessary to have, for each wave length, two phase plates constructed so that when one has a maximum or minimum for a certain φ-value the other has its intensity value on one of the steep parts, Fig. 15. This can be done by choosing the position for O′ (cf. section 2.2) in a suitable way, e.g. ψ about $\pi/2$ and $3\pi/2$.

In order to be able to measure the dispersion, it was moreover decided to measure with at least one more wave length than the green mercury line used previously

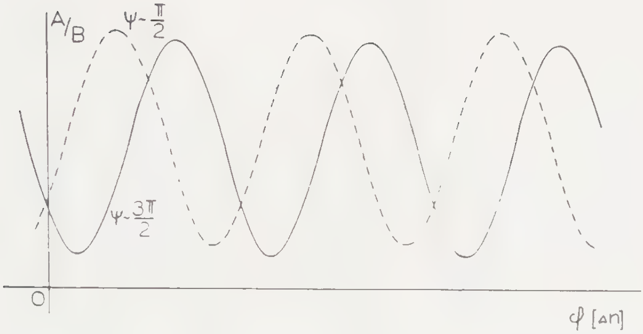

Fig. 15. The intensity ratio in the image as a function of the relative phase differences in the object for two phase plates with steps corresponding to about $\pi/2$ and $3\pi/2$.

(1, 2, 3, 4, 5)—a strong blue line was therefore chosen. This would require altogether four phase plates but only three could be incorporated in the instrument. It is possible to use one of the plates for two wave lengths by letting the step of the plate correspond to different multiples of 2π plus a smaller angle for the two wave lengths so that the desired ψ-values are obtained according to section 2.1. Such a procedure was, however, not employed in the present instrument. The three phase plates, two for the green line and one for the blue, were placed close to each other. As the intensity ratio is very sensitive to changes in the position of the plates, they are fixed and the entrance slit imaged on them. The selection of a certain phase plate is made by moving a shutter in front of the slit inside the monochromator.

The cell, slits and phase plates are all placed vertical so that, when the instrument is used for liquids, the liquid samples in the cell can be easily changed.

3.1.1 *The monochromator*

The monochromator has a plane grating in an Eagle mounting, Fig. 16. It has two entrance slits, thus making it possible to measure at the two wave lengths simply by moving a shutter. Light from a special mercury lamp *La* is focused on the entrance slits Sl_1 and Sl_2. The light from the slits goes via the mirrors M_1 and M_2 to the grating *G*. Two spectra are focused on the exit slit Sl_3 so that the blue light from Sl_1 covers a little more than one third of its length and the green light from Sl_2 a little more than the remaining two thirds. All slits are made of 30 mm long razor blades mounted on jaws. Each jaw is fixed to the base plate of the slit with two parallel blade springs. By means of a micrometer screw, the jaws can be pushed down and the slit opened symmetrically. The slit width can be varied reproducibly from a few microns to about 0.6 mm. The mirrors M_1 and M_2 have fine adjustments for both turning and lateral movements along the axis of the incident light, so that the angle of incidence for the grating can be adjusted. The grating holder allows as usual adjustment around three axes. All other optical parts in the monochromator can also be adjusted. The shutter *Sh* and spectral filters *F* are mounted together in front of the exit slit Sl_3. They can be moved along a slide block. The shutter screens the light in each of its three different positions so that only 9 mm of the slit is used at each time. The spectral filters (Schott und Genossen) are for the green mercury line, 5461 A, and the blue line,

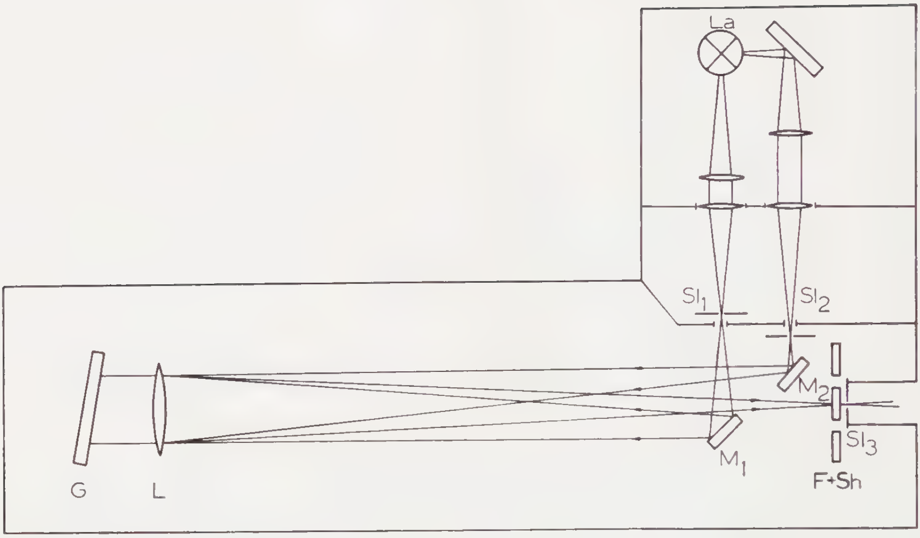

Fig. 16. The monochromator. For notations, see text.

4358 A. They are placed in this position at the shutter so that they can absorb all unwanted blue or green light and stray light from the grating and other optical parts. The shutter at the exit slit could have been combined with a shutter at the entrance slits but that would have complicated the mechanical system and the filters would still have been required for removing stray light. The lens L has a focal length of 600 mm and the grating has 720 grooves/mm so that a sufficient separation of the blue lines 4347 and 4358 A is achieved, cf. sect. 5. All details in the monochromator unit are mounted on a stable iron base plate.

3.1.2 *The refractometer part*

The refractometer part is seen in Fig. 17 which is more detailed than the schematic Fig. 1. The light from the monochromator Mo is made parallel by means of the first lens L_1 and, after its passage through the cell O, it is focused by the second lens on the phase plates Ph. The two lenses are corrected for the two wavelengths 5461 A and 4358 A so that they have the same focal lengths (914 mm). They have an aperture of about 1:20 and thus the desired low value for the spherical aberration is obtained. Each phase plate is 10 mm wide. They are mounted in a holder so that their surfaces are in the same plane and so that the phase steps form a straight line with a tolerance of a few microns. (Since this alignment is rather difficult, it is best to make all plates on the same glass substrate and, in the manufacturing procedure, mask two thirds of the surface when each of the different steps are made.) The holder can be rotated round the axis of the incident light for the central plate. A displacement in the $\varkappa$-direction is made by means of a sliding movement. The micrometer screw that controls this movement is furnished with a gear box having spring-loaded wheels. The reproducibility of this adjustment is better than half a micron.

After the phase plates comes a lens L_2 that gives an image of the object with a mag-

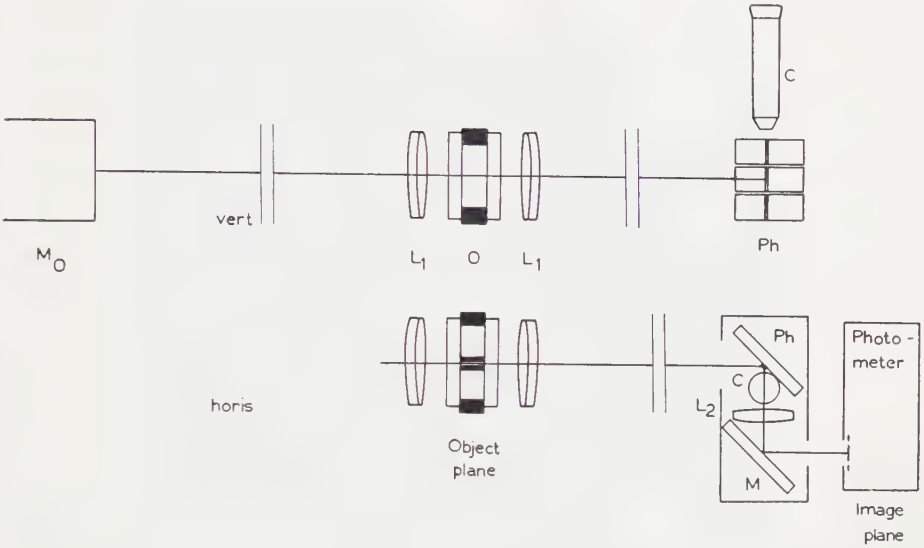

Fig. 17. Schematic drawing of the whole arrangement in two projections. For notations, see text.

nification of about 0.24. It can be moved in two directions so that the image on the photometer slit can be aligned correctly. The mirror *M* is an auxiliary mirror used for directing the light beam to the image plane in the photometer unit.

The diffraction pattern on the phase plate can be studied with a microscope *C* that is furnished with mirrors so that the light is reflected into it when it is moved down into the light beam. Visual focusing and adjustment of the phase plates are made using this microscope.

3.1.3 *The cell and its holder*

The construction of the cell depends on the sample to be measured. For gases and when a high sensitivity to refractive index differences is wanted, a long cell should be used. For liquids, the demands on the temperature constancy in the cell puts a limit to the usable length. In this investigation, a 30 mm cell was chosen since it gave sufficient accuracy. (Even shorter cells could have been used because the accuracy in the readings was higher than the reproducibility of the samples, cf. section 8.) The cell is seen in Fig. 18. It has a metal part consisting of two halves with three openings, cf. Fig. 1. The central opening is 1.3×20 mm^2, the bars 1.2 mm thick and each reference area 20 mm square. The windows are 12 mm plane parallel glass plates of optical quality fixed to the cell with small amounts of paraffin wax. The metal halves which are screwed together, are also tightened with paraffin wax. The cell is made of pure silver and all walls and channels in it are shaped so that all bubbles automatically disappear through the outlet tubings on the top when the cell is placed vertically and filled with liquid. The flexible teflon tubes are connected to the cell using nipples of nickel. In the sample part of the cell, a micro stirrer is placed so that small bubbles sticking to the walls when the liquid is changed can be removed and,

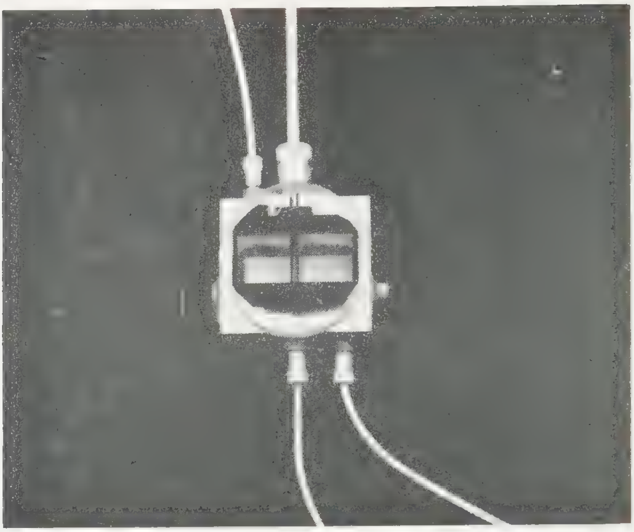

Fig. 18. The cell. Note the masks on the windows which prevent reflections from the surfaces inside the cell.

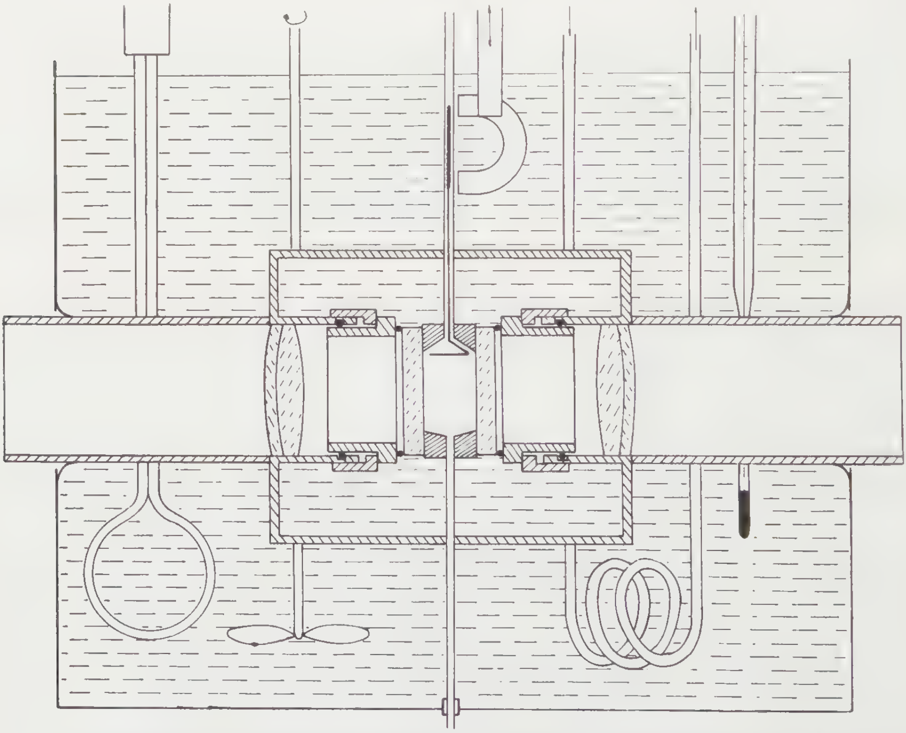

Fig. 19. The thermostat with thermometers, heating and cooling devices, stirrer and cell holder. The micro stirrer in the cell is actuated by means of a magnet.

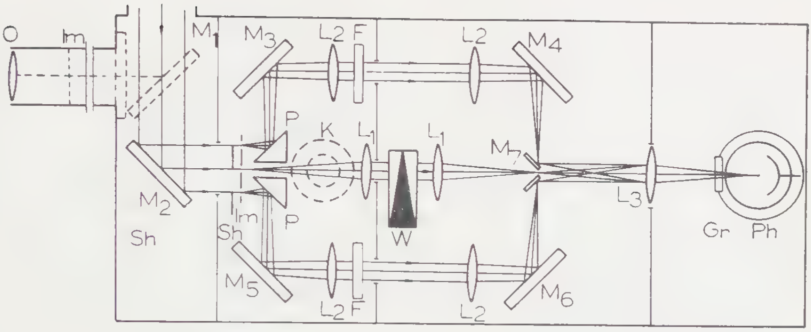

Fig. 20. The photometer part. The reference light corresponds to the upper and lower beams and the sample light to the middle beam.

also, so that a uniform temperature can be obtained faster. The stirrer is made from a nickel wire and a short nickel rod and is actuated by a magnet, Fig. 19.

The cell is placed in a holder in a thermostated bath, Fig. 19. Between the cell and the lenses L_1, Fig. 17, there are tubes with O-rings that are pressed against the cell and hold it in a fixed position. The space just outside the cell and between the lenses is very sensitive for phase differences. It is therefore not possible to allow the water in the bath to fill this region. The air here and outside the lenses in the tubes is held at constant temperature and does not give rise to striae.

The thermostating bath consists of two containers (cf. Fig. 19). The temperature in the outer bath is kept constant to some hundredths of a degree by means of a contact thermometer, an electronic relay, a dip heater and a tube with circulating cool water. By means of a thermostatic device, the room temperature is also held at the same temperature as that for the bath. The temperature in the inner container has been measured with thermocouples and its variation is of the order of ± 0.004°C. The temperature in the inner cell has, of course, an even higher constancy and it has proved to be sufficient for the measurements on heavy-light water solutions, cf. the measured temperature dependence, section 9. The temperature is determined using a calibrated thermometer in the outer bath.

3.1.4 *The photometer*

The photometer described earlier by the author (2) has been rebuilt. As discussed in section 2, the intensity ratio is measured for the central area relative to two equal areas, one from each of the reference fields. The phase contrast image of the cell falls on a triple slit *Im*, Fig. 20. Three equal areas corresponding to about 0.8 of the total central area are taken out. The light from the central area passes, as a parallel beam, through the gray wedge W and is then focused with unit magnification between the two mirrors M_7. The light beams from the reference areas are reflected at the prisms P which are coated with aluminium. After passing through a few lenses and mirrors, this light is focused on the edges of the mirrors M_7 so that the images of the three slits are as close together as possible. The lens L_3 then transports these images to the sensitive area of the photomultiplier cell *Ph* in such a way that the same area is used for each of them since the sensitivity of the photocell varies over its area. This

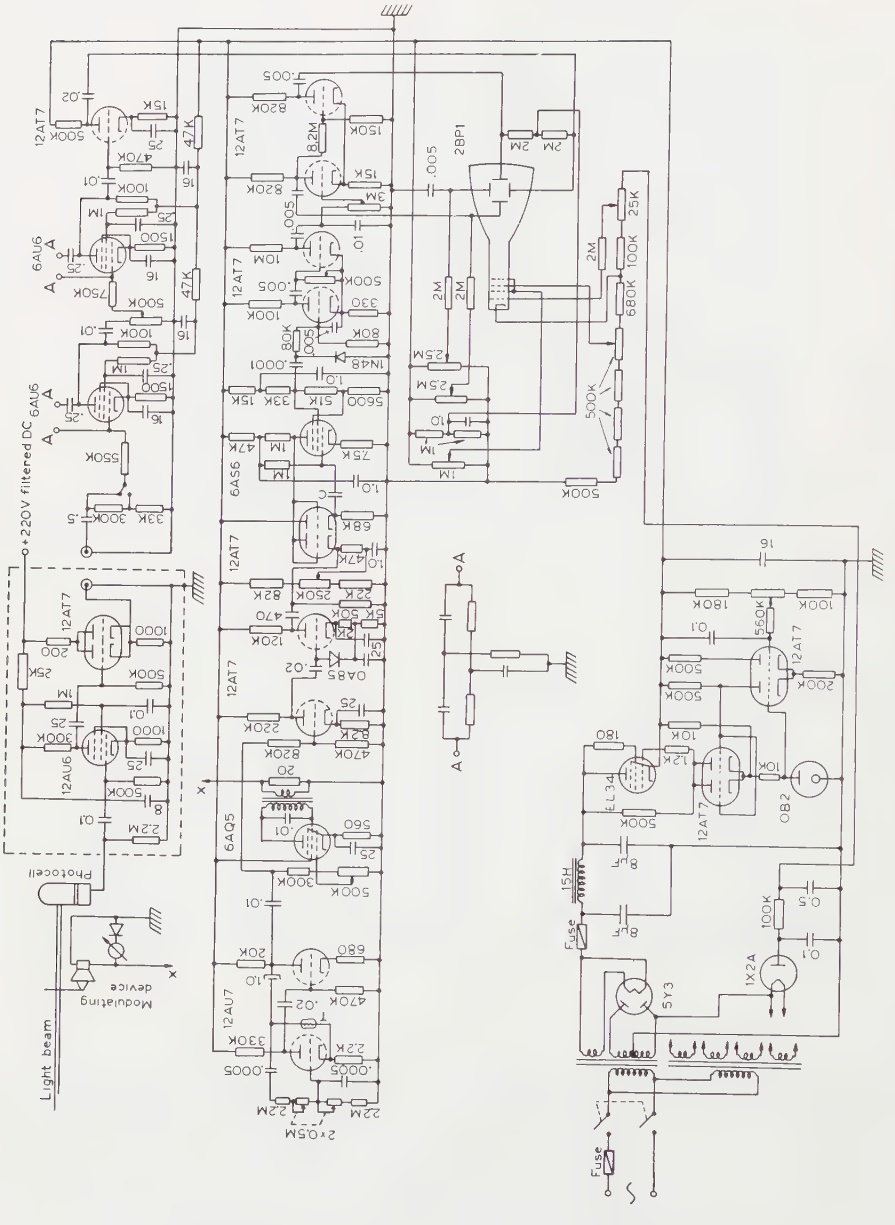

Fig. 21. Electronic circuit in the photometer system.

is achieved by means of a small defocusing and by placing a slightly ground glass *Gr* in front of the photocell. The housing round the cell is painted white inside so that part of the light which is scattered by the ground glass will, after reflection at the walls, reach the cell. The loss of signal due to the ground glass is about 50 %. By putting a mirror M_1 into the beam, the phase contrast image of the cell can be controlled in an ocular O. The position of the image and of the shutter Sh relative to the triple slit can be seen in a microscope K which can also be inserted into the light beam. All slits are seen when the prisms P are lowered, otherwise only the middle slit is observed. All optical parts have separate adjustments relative to the base plate of the photometer unit. The whole unit is mounted on a slide block, the direction of the movement being parallel to the incoming light so that focusing is easily performed.

As in the previous arrangement (2), the reference beam and sample beam fall alternately on the photocell. They are modulated with a vibrating shutter Sh. The gray wedge W is then moved into or out of the sample beam until the signal from the photocell viewed on an oscilloscope tube consists of only noise. The light intensities will then be matched. As there are some minor errors in the electronic circuit previously published (2) and since it has been moreover partly redesigned, the new circuit is shown in Fig. 21.

The light intensity for the central area and the reference areas both have a sinusoidal variation, cf. section 2. From the construction of the photometer, it is obvious that it is only possible to match the light intensities when the light from the central area is stronger and, consequently, a rather large part of the period of φ cannot be used for measurements, see e.g. Fig. 2 in which the intensity of the reference area is proportional to the square of $O'A$. However, by placing gray filters F in the reference beams, a larger part of the period of φ can be used. Because it is the steep parts of the φ-curve, Fig. 15, which are used, the filters are given such a transmission that the minima of this curve are excluded. Incorporating them would have given an unnecessarily low signal level from the photocell. The filters used have a transmission of about 15 % and this gives a DC signal of the order of 10^{-7} amp from the photocell when the modulating shutter is in its rest position, i.e. half of the light from each of the three slits reaches the photocell.

The limit of the accuracy in the matching of the light intensities is set by the noise from the photomultiplier and from the discharge in the mercury lamp. The modulation frequency is approximately 135 c/s. A mercury lamp fed by AC has its light modulated by double the line frequency, 100 c/s, and in this case there would be a cross-modulation between the frequencies 100 and 135 c/s which would give the signal on the oscilloscope tube a more noisy appearance than if the lamp was fed by DC. Tests have shown that the spread in the readings of the drum position of the micrometer screw which controls the position of the gray wedge W is, for a lamp fed by DC, about half the spread for an AC-lamp. This is the reason why a DC-lamp is employed in the present apparatus. The spread in the readings is 0.01–0.02 mm which, with the density constant chosen for the gray wedge, 0.12–0.13/mm length, corresponds to an intensity match of 0.3–0.5 %, cf. (2).

The modulation shutter has, as mentioned, its rest position so that it covers half of each slit. However, the linkage system that connects it to the driving system, viz. a small loudspeaker cone, can alter this rest position slightly. A low amplitude on the shutter would then give a signal even if the light intensities were equal. By giving the shutter a suitable amplitude, this error can be avoided.

3.1.5 *The mounting of the apparatus*

The different parts of the instrument which are described in the previous sections, are each made as separate units. They are then mounted on a bench, the monochromator and the cell holder in fixed positions and the holder for the phase plate and the

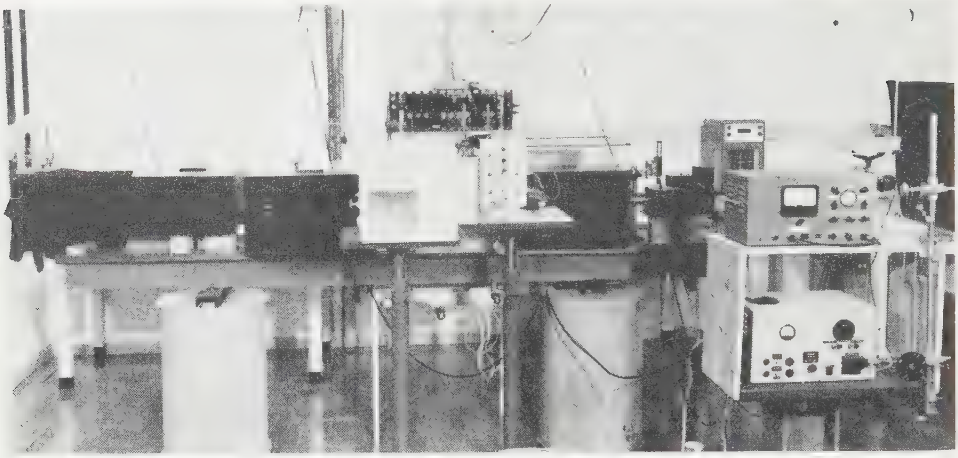

Fig. 22. Photograph of the instrument.

photometer on separate slide blocks. The distance between the exit slit of the monochromator and its image on the phase plate is about 200 cm. The tolerance for the movement of the image relative to the phase plate is ±2–3 microns. The optical axis is 20 cm above the upper surface of the bench. The tolerance in the movement of the image of the slit thus corresponds to a torsion of the bench for this 200 cm length of about 2 3 arc seconds. The system must therefore be very stable. The bench chosen is of cast iron (in one piece) commercially available and intended for use in workshops. It is 300 cm long and 18 cm wide. The upper plate is 40 mm thick and is supported by several walls, 12 cm high and 18 mm thick, the total height of the bench thus being 16 cm. The bench rests on two concrete pillars, Fig. 22, with three rubber damping pads to eliminate vibrations from the floor. On one of the pillars, the bench is placed on a short bar under which two of the pads are situated. At the other end, the bench rests on a steel ball lying on the third damping pad. In this way no auxiliary moment can be transferred to the bench. Tests showed that a slight pressure on, for example, the top of the thermostat bath produced a torsion which gave a visible change in the contrast in the image. With the present arrangement, however, no trouble has come from the bench.

The different parts in Fig. 22 are, from the left, the monochromator, a box for screening off the light in the room, the cell holder in the thermostat bath, another screening box and then the phase plate holder and the photometer unit with the arrangement for reading the drum position. In front of the instrument, there is seen a dry box used in the heavy-light water measurements and a vacuum-pressure system to facilitate the changing of samples. To the right, the electronic system can be seen.

4. Adjustment and testing of the instrument

The adjustment of the instrument must be done very carefully. The final alignment of the monochromator is made using the knife-edge technique. The exit slit, Fig. 16, is held open in a fixed position. By moving M_1 or M_2 a little, the image of Sl_1 or Sl_2 is

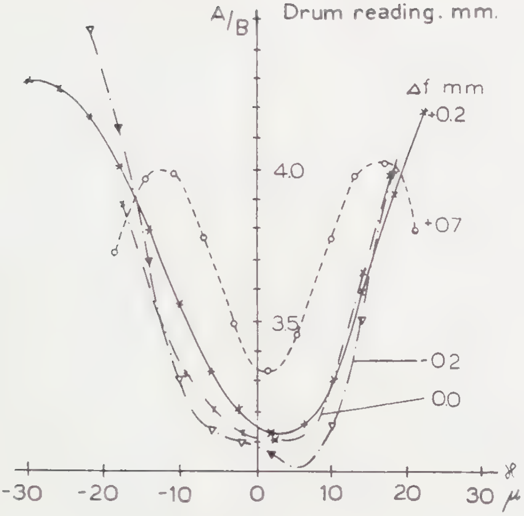

Fig. 23. Effect of the focusing of the diffraction pattern at the phase plate on the intensity ratio when the phase plate is moved sideways. The A/B-scale is divided as in Fig. 13.

made to sweep over the jaws of this slit. The changes in the light observed when looking at the grating surface through the slit are used as an indication of correct alignment. The two entrance slits and the mirrors M_1 and M_2 are moved along their respective slide blocks until, for both wave lengths, the light appears and disappears as evenly as possible over the whole of the surface of the grating.

The next step is the determination of the position of the cell holder and its lenses. This is done by means of autocollimation in which the cell is replaced by a mirror.

The positions of the phase plates and the photometer are determined first visually and then, in the final stage, by measuring the variation of the intensity ratio in the image as a function of the displacement of the phase plate at right angles to the incident light. The best focusing of the light on the phase plate is difficult to determine visually since the image of the slit is not very sharp due to diffraction. However, by measuring curves as in Fig. 13, the best position of the phase plate can be determined. Fig. 23 shows four curves with a small change of focusing between them (the focal length of the lens is 914 mm). The lowest curve is asymmetrical which must be due to asymmetry in the system, e.g. the boundaries of the phase step are situated unsymmetrically, cf. Fig. 1. The best focal setting corresponds to the curve which has a broad minimum with a value not changing by more than a few hundredths of a millimeter in the drum reading. The setting corresponding to the second curve from the bottom is chosen. Curves like this had to be determined for all three phase plates and it turned out that the best focusing position was the same for all of them. The alignment of the phase steps so that they were parallel to the image of the entrance slit was made in the same way by rotating the plate holder and measuring, for all three plates, curves like those in Fig. 13 until the minima of the respective curves were in the same position along the displacement coordinate. This adjustment of the minima positions could not be achieved better than to within 2 microns. This was, however, sufficient.

The position of the image on the photometer slit is determined in a similar way. The focusing is made visually. The intensity ratio is then measured as a function of the position of lens L_2, Fig. 17, the lens being moved by means of a micrometer screw. The curve has, depending on the q-value, either a flat maximum or a flat minimum, the width of which corresponds to a change of 0.04 mm on the micrometer screw. The mid position is chosen.

During extensive measurements with the apparatus, which were performed over several months, these adjustment curves were checked repeatedly to make certain that the instrument did not change. The curve for the photometer was measured at rather long intervals but the one for the phase plate was checked more often since it has smaller tolerances (about a tenth of the former). By comparing the positions of the steep parts of the latter curves taken on different days, changes of the order of 0.5 μ could be detected in the position of the slit image on the phase plates. The variations from the chosen position were mostly of this order, and, as they had no influence on the measurement and calibration of the instrument, they were not compensated for. On some occasions, the change was as much as 2 μ. The position was then readjusted although it was not absolutely necessary. In this way, errors in the measurements due to any possible mechanical changes in the instrument could be controlled so that they were less than the error from the matching of the two light beams in the photometer.

5. Interferometric properties of the lamp and monochromator

In all interferometric measurements, the upper limit of the measuring range is set by the monochromaticity of the interfering light amplitudes. Since the interferences in the phase contrast refractometer are of the same kind as in ordinary Michelson, Twyman and other two beam interferometers, the decrease in contrast with the number of interfering wave lengths follows the same law. By contrast or, using an older term, visibility, we mean here the ratio $(I_{\max} - I_{\min})/(I_{\max} + I_{\min})$. (The interfering amplitudes are, see section 2 Fig. 2, the amplitudes $O'A$ and AB.) This problem has been treated by several authors since Michelson (14) and, especially for the case of phase contrast, by Ingelstam (15) in connection with the determination of the natural line width of spectral lines. As upper limit for the measuring range of the present instrument, a decrease in the contrast of 0.5 % is chosen since it corresponds to the precision of the photometric measurement. This limit must lie above an interference order of 275 for the green 5461 A line and 360 for the blue 4358 A line to make it possible to measure the whole heavy-light water system with the chosen cell.

The properties desired for the lamp are: To satisfy photometric demands, it should have a high luminance and be fed by DC. For interferometric purposes, however, it should have a narrow line width and negligible background. The first condition would require a relatively high pressure in the lamp whereas the second necessitates a low-pressure lamp. The shape of the 5461 A line for several mercury lamps of low and medium pressure has been recorded in a spectrometer by photoelectric scanning and registering of the line. The lamp chosen is a special mercury lamp made by the Swedish lamp factory Luma at their Research Laboratory. It consists of two bulbs with one electrode in each and an approximately 40 mm long, narrow tube between them. The position of the discharge in this narrow tube is very stable. The lamp can be fed by DC. An examination of the line shape at different powers shows that this lamp gives a higher intensity and less self-reversal of the line than other lamps at the same effect. The band width is also smaller. The lamp can be fed with up to 150 watts (self-reversal begins at about 100 watts). Since the band width increases with the power, the lamp is, as a compromise, usually run at 85–90 watts. The half width is then less than 0.4 A.

A calculation with formula (17) Ref. (15) assuming this band width for both lines indicates a decrease of 0.5 % at 1300 periods for the 5461 A line and 1030 for the 4358 A line. However, the formula used is an approximation that neglects the background around the line. Although the background is of low intensity, it has an appreciable influence on the decrease because it is integrated over a large spectral interval. It was thus decided to make an experimental investigation of the usable interference order. (Earlier experience using a lamp with a half width of about 1.1 A together with a monochromator with band width of 10 A indicated a larger decrease than 0.5 % at interference orders less than 100.)

The monochromator had to be given such a dispersion that the weaker line 4347 A was well separated from the strong line 4358 A. For the chosen grating with 720 grooves/mm and the lens of 600 mm focal length, the dispersion is $d\lambda = 2.3 \times 10^{-2}\, ds$ where $d\lambda$ is in Angstrom and ds the distance in the spectrum in μ. The separation of the lines is thus 435 μ which is sufficient for present purposes.

5.1. *Interferometric tests*

5.1.1 *Interferometric test with the refractometer*

A 100 mm cell was placed in the refractometer instead of the usual one and the instrument adjusted. The gas in the sample cell was then slowly evacuated and the intensity for this area in the phase contrast image recorded using the photomultiplier and a Leeds and Northrup photocell recorder. Since intensity fluctuations in the lamp could not be compensated for in this investigation, each curve was taken three times and the contrast calculated from the sine-shaped recordings, cf. Fig. 15. The gas used should have a high refractivity and must not react chemically with the parts in the cell. Suitable gases are N_2O and C_2H_2, both of which were used, N_2O for the first few measurements and C_2H_2 for the remainder since it has a higher refractivity.

For the green 5461 A line about 90 periods were obtained. The contrast for ten periods in the beginning and end of each recording was calculated and thus each value in Table 1 is the mean of 30 periods.

Table 1. Interferometric contrast for interference orders up to 90 for $\lambda = 5461$ A.

Entrance slit of the monochr. microns	Band width A	Mean contrast for the first ten periods %	last ten periods %
100	2.3	90.0	89.9
300	6.8	89.9	90.0
550	12.5	89.9	89.9

Table 2. Interferometric contrast for interference orders of 110, $\lambda = 4358$ A.

Entrance slit of the monochr. microns	Band width A	Mean contrast for the first ten periods %	last ten periods %
100	2.3	69.1	69.1
300	6.8	69.2	69.3
550	12.5	69.2	69.3

With the blue 4358 A line, about 120 periods could be recorded and the result is shown in Table 2.

The values in the tables may possess errors from fluctuations in the recordings and from the calculations—an error of 0.1 mm in the value of the minima in the curves for Table 1, which can come from a faulty determination of the zero line of the record, gives an error in the contrast of 0.14 %. The difference in the contrast values in Tables 1 and 2 is due to the fact that the phase plates have different properties, cf. section 2. From the tables it is clear that for these two spectral lines there is no fall off in the contrast for these interference orders even when the band width is 12.5 A. With a narrow entrance slit, which corresponds to a small band width in the monochromator, the light in the solid angle at the excit slit will be uneven due to optical imperfections and, in addition, the demands on the mechanical stability will be high. On the other hand, nothing is gained by using unnecessarily wide entrance slits. The slits in the monchromator were therefore chosen to be 150 μ wide corresponding to a band width of 3.4 A. Thus, all the light in the line is transmitted and the background effectively cut off. This means that higher interference orders can be used. (This experiment was performed before the measurements on D_2O solutions were started. It was, at that time, not intended to use higher concentrations than about 30 % D_2O.)

5.1.2 *Interferometric test with a birefringent interferometer*

In order to get the whole curve for the contrast as a function of the interference order of the monochromator and lamp, the light from the exit slit was examined with a birefringent interferometer built by Ericsson and Sjöfall at this laboratory (16). The exit slit of the monochromator was imaged on the entrance aperture of the interferometer. The interferences were obtained between light reflected from different gauge blocks, the instrument thus giving the contrast for fixed interference orders. The following steps for the gauge block were chosen: 20, 50, 110, 300, 500, 1100, 2000 and 4000 microns giving the interference orders 74, 184, 405, 1105, 1840, 4050, 7360 and 14 700 for the green line 5461 A. The interference pattern was photographed with Agfa Isopan Ultra film, the exposure time being several hours. The film was photometered and the contrast values evaluated, cf. (16). Four different exposures were used and the result is shown in Fig. 24 with the interference order on a log scale. The relatively large spread in the values is due to the photographic procedure but the mean curve gives a good indication of the contrast function. The fall off at 1100 periods is about 1 %.

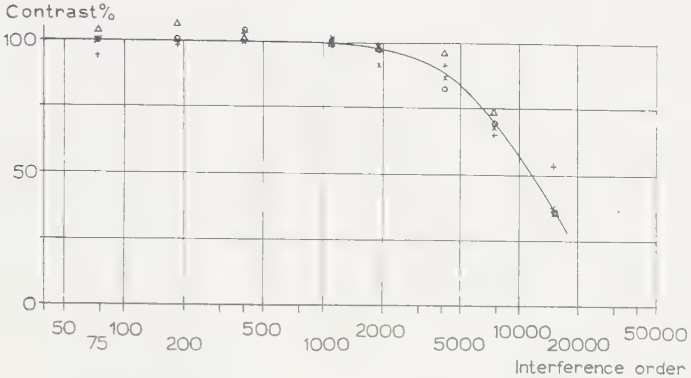

Fig. 24. The contrast of the interference fringes as a function of interference order for the lamp and monochromator, $\lambda = 5461$ A. The determination was made using a birefringent interferometer.

5.1.3 *Discussion of the result*

The experiment in the preceding section was only made with the green line 5461 A due to experimental reasons. The two lines 5461 and 4358 A are transitions from the energy level $7\,^3S_1$ to $6\,^3P_2$ and $6\,^3P_1$ respectively. The difference in their natural line widths depends only on the different mean life time of the last two levels. The hyperfine structures for the two lines are similar. However, at the actual temperature and pressure in the lamp, the broadening of the lines due to the Doppler effect and pressure broadening predominate so that the influence of other effects can be neglected (17, 18).

The Doppler width of the line is, see e.g. (17), proportional to the wave length and thus the decrease in contrast for the interference pattern is independent of the wave length. The effect of the pressure on the line gives a broadening of the half width which is independent of the wave length. The influence of this effect is therefore the same on the two lines because they are emitted in the same discharge. The half width of the 4358 A line is thus smaller than that for the 5461 A line but not in the relation of the wave lengths. In the calculations, the same half width is assumed (this being probably an upper limit for the 4358 A line).

Determining the constant in formula (17) Ref. (15) so that the contrast has fallen by 1 % at N = 1100 gives, for 0.5 % fall off, N = 780 for the 5461 A line and N = 620 for the 4358 A line. These values are less than those previously calculated from the scanned spectrum. They are, however, well above the necessary interference orders. In the measurements on samples corresponding to high interference orders, some of the readings happened to fall on the maximum of the calibration curve for the instrument. No decrease in these readings could be detected.

5.2 *Possible displacement of the Δn-curve due to the shape of the spectral line*

The experiment in the preceding section has shown that a certain number of interference periods can be used for measurements without a fall off in contrast of more than 0.5 %. However, at the same time as the contrast decreases, there will be a continuous change in the positions of the maxima and minima of the Δn-curve, cf. Fig. 15, from the positions for an ideal spectral line. The magnitude of this change is rather difficult to measure, it is instead calculated from the shape of the spectral line.

From Figs. 2 and 15, it is seen that the intensity I can be written $I \sim 1 + V \cos 2\pi p \nu_0$ where p is the optical path difference and ν_0 the wave number of the ideal spectral line (the origin is shifted slightly so that the intensity has a maximum for $p = 0$). To get the actual intensity, this relation has to be integrated for the spectral line over the band width of the monochromator. Using the same notations as Michelson (14), this gives

$$I = P + V \sqrt{C^2 + S^2} \cos (2\pi p \nu_0 - \delta), \text{ tg } \delta = S/C$$

P is the integral over the spectral line $\psi(\nu)$, i.e. the total transmitted intensity, C and S the cosine and sine Fourier transforms of it, $C = \int \psi(\nu) \cos 2\pi p \nu \, d\nu$ and $S = \int \psi(\nu) \sin 2\pi p \nu \, d\nu$. This expression is the same as Michelsons's apart from the factor V which depends on the fact that the interfering light amplitudes are not of equal magnitude, see Fig. 2. The Fourier transforms of the spectral line can be calculated for different p-values with an harmonic analyser and the desired angle δ is then obtained. The present author has used a mechanical analyser made by Mader-Ott, Kempten, Allgäu. The spectral line chosen for this calculation is one of the recordings mentioned previously. These recordings were made with a test lamp which had a discharge tube which was about 10 mm shorter than the lamp used in the instrument. This means that, if the two lamps are fed with the same power, the recorded line is the broader one. Evaluating the recording corresponding to 90 watts thus gives an upper limit for δ. Before the evaluations of C and S are made, the recorded spectral line should be corrected because it is a convolution of the true line and the influences of the widths of the slits and of the properties of the grating (an 1 metre concave grating) in the spectrometer used. However, the monochromator of the phase contrast refractometer also comprises a grating together with slits. The influence on the spectral line from the apparatus can thus be assumed to be about the same in the two cases, no correction of the recorded spectral line has therefore been made. The two p-values corresponding to 300 and 600 interference periods have been used. The calculations give δ less than 2° and about 3° respectively, which corresponds to less than 10^{-7} and 1.5×10^{-7} in refractive index. The values are not very accurate since the analyser gives the integrals divided by half the period length. The S-values are only slightly larger than the spread in the readings. (The above equation for the intensity could, in principle, have been used to calculate the decrease in contrast for different interference orders. However, since the arrangements in the spectrometer used for the recordings of the line and the monochromator of the phase contrast refractometer were not the same, it was decided to measure the contrast fall off curve with the actual monochromator.) For the heavy water measurements interference orders up to 300 were used. Since errors from other influences in this region were larger than 10^{-7}, cf. below, no corrections for the influences from the spectral line were made.

The results obtained in the examination of the phase contrast refractometer show that it has a measuring range for refractive index differences from a cer-

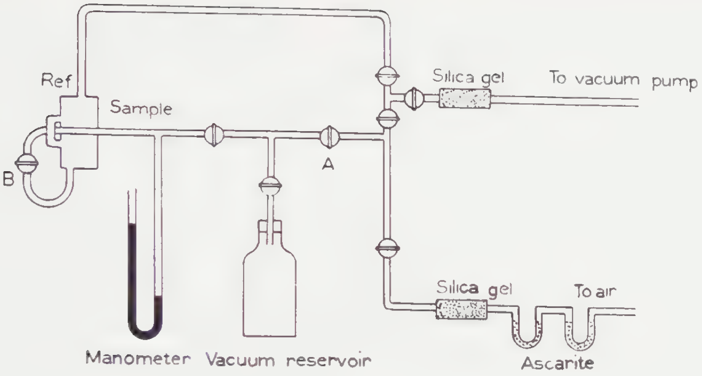

Fig. 25. The gas system. The tube marked "to air" can be connected either to out-door air or to an air-filled bomb.

tain low value, which corresponds to the accuracy of the photometer, up to about 9×10^{-3} for a 30 mm cell,—for the upper limit of the measuring range the error due to the monochromaticity of the spectral line is of the order of 10^{-7}. This range is twice what is necessary for an examination of the whole heavy-light water system.

6. Measurements on gas samples

The refractivity $(n-1)$ of a gas is, to a first approximation, proportional to the pressure. By determining the intensity ratio as a function of the pressure difference for the two parts of the cell, we get a calibration curve for Δn with equidistant slopes as in Fig. 15. From this distance between the sloping parts of the curve, the cell length may be calculated since the refractive index for the gas, e.g. air, is well known (19, 20). The air is taken from outside the building by means of a tube and passes through a purification system illustrated in Fig. 25, cf. (19). The system has been used for several years and was also employed for the measurements in the infrared wave length region (6).

When measuring the slopes, the cocks A and B are closed so that more and more air can be evacuated from the sample cell. The reference cell is connected to the open air. It was, however, found that the slopes were not parallel. At the end of the measurement, the cock A was opened. The pressure difference in the cell disappeared and the zero position was determined. This had also changed and it was found, at repeated measurements, that the change was always in the same direction. By letting air stream through the cell for some minutes, the former zero position was obtained. In order to examine this change, which can be due to a gasing material in the system, all connections and nipples at the cell were removed. Both the sample and reference volumes were therefore connected by only short tubes to the air in the room and thus the diffusion of the air in and out was not hindered. Measurements of the zero position during several days now showed no change. There was thus no drift in the instrument. The error can possibly be due to changes in the air as reported by Tilton (21) but that effect was over longer periods of time and is therefore not so probable in this case. The room was thermostated so the effect cannot come from temperature differences. It is thus most probable that some material in the system gave off gas.

In the search for the gasing material, all rubber tubings were removed and short teflon tubings and stainless steel tubes used to connect the cell to the air purification system which was made of pyrex glass. It was found, however, that the effect was not removed. An examination of the influence of silica gel and Ascarite gave no result. These experiments indicated that the phenomena probably occurred in or near the cell. In order to test this assumption, the cell was filled with fresh air and the zero position determined. All tubings were then closed near the cell. After a few hours, the cock B was opened and a reading taken. A drift in the zero position of the same order as before was obtained. Flushing the cell with new gas gave the former zero value. The experiment was repeated several times for the sake of verification.

Since air is a mixture of different gases and since the surface areas in the reference and sample parts of the cell are not in proportion to the volumes, the drift can be due to adsorption instead of gasing in the cell. This was tested by using nitrogen. The same drift as before was obtained which indicated that the effect was not due to adsorption in the cell.

If the gasing of the material in the cell had given the same change in refractive index in both parts, no drift would have occurred. In order to determine separately the change for each of the cell chambers, the cell was flushed in two steps after it had been allowed to stand for some hours with the tubings closed close to the nipples. First, the reference part was examined and then the sample part, zero values being determined before and after each flushing. (Before flushing the cell chambers, the tubings were always flushed with fresh air for several minutes.) From these values, the drift after three hours for the sample cell was found to be about -1.6×10^{-7} in refractive index and for the reference cell about a quarter of this value. The sensitivity of the instrument was about 1.5×10^{-8}. An estimate of the ratio of the lengths of the tightenings for the two cell parts in relation to the respective volumes showed that the length of the tightenings is about four times longer per unit volume in the sample cell than in the reference cell. This indicates that it might be the paraffin wax which gave off gases. Tests with high vacuum silicon waxes instead of paraffin wax gave, however, a drift of the same order. The ratio of the surface areas relative to the volumes also gave about the ratio mentioned above. These experiments have given much valuable experience, although they have not given any new results. They have shown how difficult it is to keep the gas in such small volumes under absolute control (the sample volume is about 2 cc and the reference volume 27 cc). The drift from one day to the next was about 2.5×10^{-7}. This means that the relative change in $(n - 1)$ for the air is less than 1/1000 because $(n - 1)$ is about 3000×10^{-7}. Since the gases that can come from the paraffin wax are hydrocarbons, they have $(n - 1)$ values several times the value for air. The change in the air composition is probably appreciably less than 1/1000. To enable measurements on gases with an accuracy of 1.5×10^{-8}, it seems to be necessary either to find better materials or to have such large volumes relative to the tightening lengths, surface areas etc., that the influence of any eventual gasing and adsorption by the material is less than the sensitivity of the instrument. In the measurements on liquids, no drift of this kind in the readings was obtained.

The author has reported these unexpected findings concerning the high-precision refractometry of gases mainly for the guidance of other workers in this field.

II. DETERMINATION OF THE REFRACTIVE INDEX OF HEAVY-LIGHT WATER SOLUTIONS

7. Experimental procedure

7.1 *Earlier investigations*

When heavy water was discovered in the 1930s, its physical properties were examined and some of them were used for the analysis of heavy-light water solutions. The refractive index difference was measured using various types of instruments. Rayleigh interferometers were used by Crist, Murphy and Urey (22), Lewis and Luten (23), Luten (24), Hall and Jones (25) and others. Hall and Jones used a 100 cm interferometer cell and had a sensitivity of $2 \cdot 10^{-8}$ but temperature variations in such a very long cell must have decreased the accuracy appreciably. They used the instrument only in the low concentration region for determining the composition of ordinary water and published no refractive index values. Hollow prisms in conjunction with precision spectrometers have been used by, amongst others, Tilton and Taylor (26) and a double hollow prism by Stokland (27). The results of these and other measurements have been recalculated and published by Kirshenbaum (28) using the latest value of the specific gravity for pure D_2O. However, the accuracy in the refractive index measurements gave a lower accuracy for the analysis of D_2O-H_2O mixtures than gravimetric methods with pycnometers and floats. They have therefore not been used since the 1930s. With the new optical technique, e.g. the Riken interferometer described by Namba (29), and used up to 6 mol per cent D_2O, and the phase contrast refractometer reported from this laboratory (3), it is possible to make analyses with an accuracy of about 0.002 mol per cent which is of the same order as that given by the other methods.

7.2 *Calibration of the instrument*

The instrument must be calibrated so that the following is known, namely, the refractive index difference that corresponds to one wave length difference in optical path for the sample cell relative to the reference cell and, in addition, the calibration curve, i.e. the setting of the drum for the gray wedge in the photometer as a function of the refractive index difference within this interval. The first relation is calculated from the thickness of the cell while the latter is measured with known solutions. The refractive index for a sample is then obtained as the sum of the refractive index of the reference medium and a number of whole wave length periods together with the fraction of a period determined from the photometric measurement. By making measurements on gases with known refractive indices, cf. section 6, it is possible to determine the cell thickness and, in addition, if measurements are to be made on gases, the calibration curve within one period can also be obtained. If, however, measurements are to be made on liquids, two factors that have great influence on the calibration curve must be carefully checked. If the metal part of the cell is not absolutely plane parallel, the cell will act as a wedge with different refractive powers for substances with different refractive indices. This means that the image of the entrance slit on the phase plate will be moved and will have to be readjusted. This can, however, be done with the necessary precision. If the glass plates or lenses which are the windows of the cell are not plane, they will act as a lens of varying refractive power and thus influence the focusing of the entrance slit on the phase plate. The calibration curve is very sensitive for such changes—the maximum and minimum values changing considerably. It is difficult to readjust the focusing with the required precision. It is therefore necessary to determine experimentally the calibration curve using in the cell a liquid or a gas which has a refractive index that is very close to the index for the substance to be examined. It is preferable to use the same substance in the reference cell for the calibration and the actual measurements since the optical alignment of the instrument will then remain unchanged. In the previous determination of the D_2O-H_2O system up to 4 mol per cent (3), the calibration of the instrument was made using air and can therefore suffer from the systematic errors mentioned above. The values obtained in that determination do not agree with the present ones although they actually happened to fall on a straight line. There were, in addition, too few samples to give a satisfactory function of Δn versus D_2O concentration.

An examination of the cell components showed that the metal part was slightly wedge-shaped and that one of the glass plates gave 3 concentric rings when it was put in an interferometer and its surfaces tested. A change of focus of about 0.4 mm was observed visually when the cell was filled with water. Since measurements on gases, cf. section 6, did not give good results, it was decided to determine the cell thickness by comparing it with gauge blocks. The calibration curve was determined using sucrose solutions of low concentrations.

7.2.1 *The cell thickness*

For the determination of the cell thickness, the two plane parallel glass plates were marked and measured by comparing them with gauge blocks using a CEJ Microcator, S 509-9, with a range of 20 μ, each scale division corresponding to 0.1 μ. The joining of the gauge blocks was controlled interferometrically. After the thickness of the glass plates had been measured at different points, they were fixed to the metal part of the cell with a small amount of paraffin wax. The whole cell was then measured using the same procedure and the cell thickness at various points calculated. With the gauge blocks and Microcator used, each determination was accurate to within at most 0.5 μ. Since the thickness was obtained from three measurements, the error in it is of the order of 1 μ. It was found that the variation in the thickness along the slit-shaped sample cell was about 1 μ with a mean value of 29.846 mm. The thickness at the ends of the reference parts of the cell were 29.832 and 29.860 mm respectively thus giving a small liquid wedge. The above mentioned curvature of one of the glass plates, which is 0.6–0.7 μ, is smoothed out in the calculations when the figures are rounded off to whole microns. Since it is only changes in the sample cell which are indicated, it is its thickness that should be used, i.e. 29.846 ± 0.001 mm. This value was determined at a temperature of 21.7 C. A correction of the figure to 20.0°C gives a value that is about 1 μ smaller. Since the entrance slit of the refractometer is 30 mm long and since two of the phase plates are placed outside the optical axis, viz. the plate for the blue light and one of the plates for green light, there is a correction term to the cell thickness due to the light that makes a small angle with the optical axis. This increases the cell thickness. For the central plate, the relative increase is 4×10^{-6} and, for the two outer plates, it is 5×10^{-5}, the latter value corresponding to 1.5 μ. Since most measurements have been made at 20°C and since these corrections have different signs, they partially cancelled each other, the final correction being less than 1 μ. In the measurements on concentrated D_2O solutions, no systematic difference in the fraction of a period determined with the two phase plates for green light could be detected. For pure heavy water, it should have been 2×10^{-7} in refractive index. As most measurements were made on less concentrated solutions, the difference for the two plates is of the order of the measuring error so it was decided not to use different values for the cell thickness for the different phase plates. The value given, 29.846 mm, can thus have a relative maximum error of 5×10^{-5} if systematic errors are also included. After the measurements were finished, the cell was taken out of its holder and the thickness checked. No change could be detected.

The refractive index difference Δn for one wave length difference in the optical path s was obtained from the wave length of the light and the cell thickness, $s = \Delta n \cdot t = \lambda$. From the vacuum wave lengths of the green and blue mercury lines and Edlén's dispersion formula for standard air (20) which is tabulated by Penndorf (30) and gives $(n-1)_{\text{green}} = 273.16 \times 10^{-6}$ and $(n-1)_{\text{blue}} = 276.28 \times 10^{-6}$ at 20°C and 760 mm Hg pressure, the two wave lengths can be calculated for these conditions. From these values, the period lengths for $\lambda = 5461$ A and $\lambda = 4358$ A were found to be 1829.65×10^{-8} and 1460.28×10^{-8} respectively in refractive index difference.

7.2.2 *The calibration curve*

The intensity ratio for the sample area relative to the reference area as a function of the refractive index difference within a period, cf. Fig. 15, was determined by means of measurements on sucrose solutions of low concentration. The distilled water used for these solutions was always taken from the same bottle as the water for the reference volume. Six or seven concentrations could be measured each day. In order to get stable conditions and reproducible results, the water was handled as described below and kept either in Pyrex glass flasks that had been filled with water for a long time to remove all soluble matter or in polyethylene bottles. Since the maximum error in the matching of the two light beams in the photometer corresponds, on an average, to a refractive index difference of 3×10^{-8} and the period length to about 1800×10^{-8}, the concentrations of the solutions must be known to better than 1/600. (As the scale for the A/B ratio is antilogarithmic, the error in the refractive index difference, which always corresponds to the same displacement of the gray wedge, is less at the lower parts of the slopes of the calibration curve and larger at the higher parts.) Tabulated values for sucrose solutions show that a solution with 13 mg sucrose in 100 g water (concentration $= 1.3 \times 10^{-4}$) will give about one period. Since the sensitivity of the balance (Mettler BH 26) is 0.1 mg, the solutions were made in two steps. A solution with a concentration about 20 times greater than the most concentrated one required was made and then diluted accordingly. In this way, the amount of sucrose was always more than 200 mg and thus the relative maximum error was less than 1/2000. All weighings of water were corrected to dry air at 20°C and 760 mm Hg pressure. The correction has proved to be at most 1×10^{-8} in concentration units and can therefore be omitted.

About thirty points on the calibration curve were determined before the measurements on heavy water solutions were started. At regular intervals, additional points were measured in order to detect any change in the calibration. This was also done after the D_2O series had been finished. The values in the calibration curve have to be corrected for two types of drift. Each day, the experiment was begun by deter-

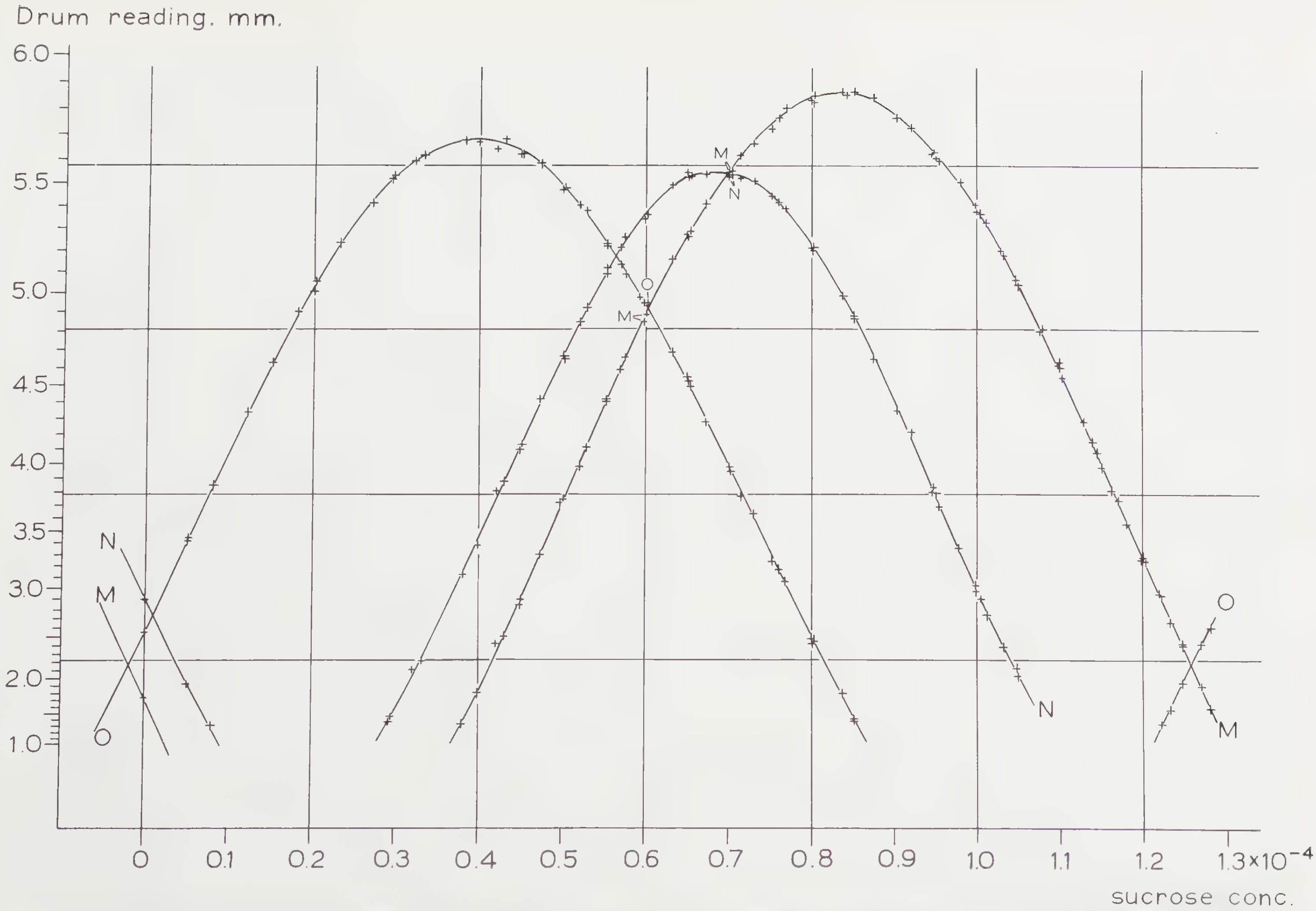

Fig. 26. The calibration curve for measurements at 20 C. The scale for the drum reading is antilogarithmic, i.e. the intensity scale is linear which thus gives the curves their sine shape. The calibrated period is the first negative one. The D_2O-measurements give positive periods. N is the

mining the zero value, i.e. with the same water in the sample and reference cell. This zero value was determined both during and after the series. A small change during the day was often observed. The maximum drift was of the order of $6 \cdot 10^{-8}$ in refractive index which corresponds to $0.01 \cdot 10^{-4}$ in sucrose concentration. This was probably due to changes in the water in the reference cell—during the 4–6 hours it was there, it could probably dissolve a slight amount of glass or metal. The other change in the zero position occurred over a longer time, 1–2 months. During this time, a continuous drift corresponding to a refractive index difference of $-5 \cdot 10^{-8}$ for the sample cell was obtained. This can be due to a change in the cell constant as glass is solved from the surfaces. With water in the cell, it corresponds to a change in the thickness of the reference cell of 70 Å more than the change in the thickness of the sample cell. An alteration of this magnitude is quite well probable. Such a change means that the calibration curve will be moved along the Δn-axis since it is only the relative phases of the light amplitudes from the cell which determine the contrast in the image. Measurements of different points, e.g. the maxima that are most sensitive to changes along the ratio axis also showed that their values had not changed. Both of these types of drift were thus corrected for by adding an appropriate amount to the sucrose concentrations and thus all drum readings will be related to the same zero position. A calibration curve is seen in Fig. 26. From the position of the different points on it, it can be estimated that the slopes of the curve are true to within 5×10^{-8} in refractive index since the distance of the individual points from the curve is of this order.

The D_2O measurements were made at two temperatures. After lowering the temperature, a readjustment of the instrument was made, mainly to find out whether it was possible to get the same calibration curve again. This was, however, not the case, the new curve being lower. The difference, which was mainly due to refocusing, was too large to allow the same calibration curve to be used for both temperatures—it would have introduced serious errors.

The sucrose used was of pro analysi quality and made by Mallinckrodt Chemical Works. From the calibration curve, we get the first term in the relation $n = k \times c + \cdots$, i.e. the refractive index as a function of the concentration, since the concentration is so low that second and higher terms in c can be neglected. The constant k was determined from the c-value for one period. For $\lambda = 5461$ Å, we found $k = 0.1434$ and, for $\lambda = 4358$ Å, $k = 0.1453$ which may be compared with the value $k = 0.144$ for the sodium D-line for a 1 % concentration given by Landolt-Börnstein (31). The agreement is quite good.

In all the calibration measurements, the same amount of care to keep the samples pure and to avoid errors was taken as in the D_2O measurements (see below).

7.3 *The measuring technique*

The technique used for the measurements on liquids was worked out during the preliminary tests before the calibration measurements were started. In order to change the liquid in the cell, the two tubes from the top of the sample and reference volumes were connected to the gas system used for the measurements on air, Fig. 25. The gas system was altered so that a small under-pressure or over-pressure from an air-filled bomb could be applied to any of the volumes. The tubes from the bottom of the cell were placed in the respective flasks containing the liquids that were to be

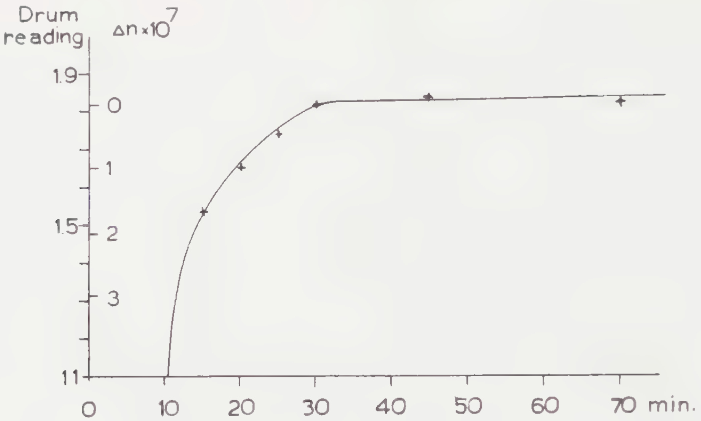

Fig. 27. Graph showing the temperature effect produced upon change of liquid in the whole cell. The time is measured from the moment the cell is full.

filled into the cell. One of the flasks was placed on a stand, see Fig. 22, so that the liquid level in it was higher than the cell. By applying a small under-pressure to the upper tubing, the cell was filled by siphoning. When emptying the cell, the liquid was allowed to run out through the lower tube. In the D_2O measurements, all handling of the solutions had to be made inside dry boxes containing Dehydrite (magnesium perchlorate). The sample cell was then emptied by applying an over-pressure to it and thus blowing out the previous sample.

In all measurements, it was necessary to wait, after changing the sample or reference water, until the temperature was once more uniform. To determine the time necessary for this, the intensity ratio as a function of the time was observed after such a change. For a change of reference water, the curve in Fig. 27 is representative. It shows that, after about 30 min, the temperature of the liquid had come to equilibrium and the measurements could begin. The time required depends of course on the original temperature difference but, as the room had a temperature very near the temperature in the bath, 30 min always proved to be sufficient. A change of the liquid in the sample cell, which has a much smaller volume than the reference cell, gave a curve of the same appearence but the equilibrium was reached in a shorter time. After about 5 min, the changes of the setting for the gray wedge were of the order of the photometric sensitivity but to be safe it was decided to wait about 10 min before the readings were taken. For each phase plate, 4–5 readings were made on the sample. Using the thermostating procedure described in section 3.1.3, no influences due to variations in the temperature could be detected during the measurements.

For the measurement of a new sample, the previous one had to be removed very carefully. With the sucrose solutions, four fillings of the cell were made with the new sample to get complete rinsing and the fifth was measured. When filling, the stirrer in the cell was actuated by the magnet so that the surface layers would be destroyed and the liquid completely changed. Each concentration was measured twice using the same rinsing procedure. If the rinsing was insufficient, these two readings were found to disagree and a third had to be made. However, it was found nearly always that this was not necessary due to the fact that the concentration differences between the samples were small. In the D_2O measurements, the same procedure was used but the first rinsing was made using only two or three fillings so the first measurement was made on a sample that had a little higher or lower concentration than the next two. All these samples were, if possible, measured three times and it was always found that the two last gave the same reading, except for highly concentrated samples, see further sect. 9.2. From the first reading, it was then possible to see whether the points were on the positive or negative slope of the calibration curve. This was especially valuable for the blue light since it eliminated one source of uncertainty—the choice between the slopes would otherwise have had to be made from the regularity of the function Δn versus concentration. For the green light with its two phase plates, the readings for them gave only one point within each period.

The relation between the refractive index n and the density ϱ of a substance has been investigated and different relations given, see e.g. Partington (32). For liquids, it has been found that the relation follows Dale-Gladstone's law, $n - 1 = k\varrho$, rather well when the density is a function of the pressure. Using the value of the compressibility coefficient for water, a calculation showed that an influence on the refractive index of the same order as the photometric sensitivity was obtained if the pressure difference is about 7 mm water, i.e. the water levels in the tubings connected to the sample and the reference cells must always be checked so they do not differ by more than a few millimeters.

8. Precautions concerning purity of the samples

8.1 *Purification of the water*

The purification procedure used for the water depends, of course, on the impurities in it. Many different methods are described by Kirshenbaum (28) and in chemical handbooks. Since the original water, ordinary or heavy, was known to contain only very small amounts of organic impurities if any, it was decided to purify it by means of three distillations. The agreement obtained between the different measurements showed that the procedure used was satisfactory. The first distillation was made with small amounts of potassium permanganate and sulphuric acid added to the water. The next was performed with barium hydroxide added and the third without any addition. Each distillation was made in different apparatuses.

All distillations, and especially the last one, were carried out slowly. To prevent any fractionation, the distillations were continued until the boiler was nearly dry.

The purity of the water was checked by measuring its specific resistivity. This method indicates, however, only inorganic impurities but, as mentioned above, it was unlikely that organic impurities existed in the original water, and moreover, the first distillation would undoubtedly have removed them. The resistivity or conductivity is usually measured with a dip electrode of platinum fed by AC with a frequency of some 1000 c/s. However, in the measurements on pure water, the parallel capacitances over the electrodes act as a shunt and thus incorrect values are obtained. To work with DC would have resulted in polarisation potentials. For these measurements, it is therefore more suitable to use AC of a low frequency for which the capacitance shunt effect is negligible. A simple resistance bridge fed by 50 c/s was used.

8.2 *Treatment of the distilled water*

The final distillation of the water was made with the water in contact with air and thus the product was over-saturated with carbon dioxide. It was degassed by boiling. The values measured for the resistivity were then 0.6–1 Megohm-cm which showed that the water was free from inorganic impurities. Water treated in this way was used as reference liquid in the cell and for making the sucrose solutions. It was found, however, that the results obtained were not reproducible. Further, it was found that water which had been stored for a long time in the pyrex flask, e.g. several weeks, did not change much during the time it was in the cell. The liquid kept in the flask had, of course, been in contact with air. Water distilled and degassed the day before was compared with this older sample of water and the refractive index was found to be $4 \cdot 10^{-7}$ higher. In order to examine the changes occurring during one day, water from the bottle that had been used for filling the whole of the cell at the beginning of the measurements was examined at various intervals. Typical changes in the refractive index were, for the water in the reference cell relative to the water in the flask, of the order of $2 \cdot 10^{-7}$ if the water was one day old and $1 \cdot 10^{-7}$ for the same water during the next day. This shows that it takes a rather long time before degassed water that is in contact with air comes to equilibrium.

When preparing the samples, it was necessary to mix the components by shaking the flasks and thus, since there was air in them, the samples became saturated with air. It was therefore necessary to stabilise the water used as reference. A carboy of distilled water was bought and this water was used as reference in all measurements and, also, for making the sucrose solutions. The heavy water solutions were made by diluting concentrated heavy water with ordinary water distilled by means of the same procedure. The ordinary water for these distillations was taken from a carboy containing the same type of water as that used for the reference cell. In the heavy water measurements, the ordinary water and the solutions were therefore measured against the same reference and the refractive index differences were calculated. When the water in the carboy had become stable, it could be assumed that its refractive index would change only very little and that it would therefore be possible to detect variations over a long period in the different distillation samples produced for the dilution of the heavy water.

The water used as reference was carefully examined. Samples taken from the carboy either directly or stored for some hours in contact with air showed differences of the order of 4×10^{-7} in n. The water kept in contact with air and then shaken in the bottle had the lowest value. The resistivity of the original water in the carboy was about 0.5 Megohm-cm which indicated that it was free from inorganic impurities and had very little dissolved carbon dioxide.

In order to stabilise the water, dry, carbon dioxide-free air was bubbled through it. The whole of the cell was filled with this water and thereafter the sample with the lowest value was measured. The latter sample still had a lower refractive index, indicating that the water in the carboy was not in equilibrium with the air. The bubbling of air was continued and measurements were performed until there was no difference between samples taken at an interval of several hours. The decrease in the refractive index could be determined from the different readings and was about 5×10^{-7}. In order to examine the effect of degassing, a little of this water was boiled and then poured into two flasks, so that one of them was quite full. Samples from them were measured and, then, the remaining liquid in the flasks was shaken with air and new samples taken. The decrease in refractive index for the water from the incompletely full flask was about 4×10^{-7} and for the water in the full flask about 15×10^{-7}. This indicates that the resaturation process is rather fast in the beginning and may be detected using instruments of lower sensitivity (33).

Using this stabilised reference water, experiments were performed to see whether any differences appeared when the water was stored in pyrex or polyethylene bottles during the day. Repeated measurements with different bottles showed no variations larger than the apparatus sensitivity, i.e. 3×10^{-8} in refractive index. No errors resulting from the storing of the water were therefore introduced.

In order to examine the reproducibility of the distillations, several distillates were treated as above by bubbling air through them and the changes in their refractive index were followed during several days. All measurements were made using reference water from the same carboy supply. The results from different days are therefore comparable and some of them are shown in Table 3.

During the time the measurements were made, the water samples were kept in pyrex bottles with relatively large volumes of air over them. The table shows that the water samples after treatment with air have a refractive index that differs from the reference water by between -13 and -26×10^{-8}. The difference for freshly distilled water in contact with air is -19 to -64×10^{-8}. This shows that, as found above, the treatment of the water with air makes it more stable. The resistivity also increases, indicating that carbon dioxide is removed.

The distillation and treatment of the water has been found to give a reproducibility for the refractive index of 1.5×10^{-7}. All ordinary and heavy water was handled in the same way. Each day measurements were made, the difference between the water for dilution and the reference water was measured. The values obtained for the difference exhibit a slight variation around a mean value of -2×10^{-7}. For the D_2O samples, the difference in n, 1.5×10^{-7}, due to the treatment is less because the refractive index of the sample is determined relative to that of the water used for dilution. It is only at high concentrations that this error can influence the n-value obtained in the investigation. If an unknown sample is to be analysed, this difference of course decreases the precision. It corresponds to ± 0.0015 mol per cent.

There are a few earlier publications which may be compared with the author's findings. Kirshenbaum, (28) p. 370, reports that degassing of the sample can introduce serious errors. He states that degassing diminishes the refractive index by about 8×10^{-7} and that, when the water is stored in contact with air the resaturation will be complete within a few hours. He also points out that freshly distilled water in contact with air should give stable and reproducible values right from the beginning and hence that, if the sample is distilled under vacuum, it ought to be thereafter saturated with air. The present author's experiments show that the degassing of air-saturated water increases the refractive index. The resaturation is rapid in the beginning but, to reach equilibrium, a long time is necessary. Tilton and Taylor (33) have discussed the effect of air dissolved in water. They used a hollow prism on a spectrometer and had a sensitivity of 1×10^{-6} in refractive index. The water was distilled under vacuum and thus freed from dissolved gases. They found a somewhat higher refractive index for stored distilled water after it has been degassed although they were not able to measure it. The sensitivity of their instrument was of the same order as the effect. From the known density difference between air-free and air-saturated water, they calculated, assuming that $n-1$ is a linear function of the

Table 3. Change in refractive index with time for different water samples.

Water	Day	Air bubbling	$\Delta n \times 10^8$	*R* Megohm-cm
W_1 dist. and degassed on 13 Jan. Stored in half-full bottle	24 Jan.		−19	1.0
		50 min, 1 l/min	−22	
		85 min, 1 l/min	−21	1.2
	26 Jan.		−20	1.1
	30 Jan.		−14	1.15
	31 Jan.		−16	1.1
	2 Feb.		−14	0.95
W_2 dist. on 19 Jan., not degassed, stored in half-full bottle	24 Jan.		−52	0.65
	26 Jan.	60 min, 1 l/min	−19	0.85
W_3 dist. on 22 Jan., not degassed	24 Jan.		−43	0.65
		65 min, 1 l/min	−32	1.2
	26 Jan.		−21	1.35
		40 min, 1 l/min	−22	1.35
W_4 dist. on 26 Jan., not degassed. Measured some hours later	26 Jan.		−64	0.48
		90 min, 1 l/min	−30	1.0
	30 Jan.		−10	0.75
W_5 dist. on 27 Jan., not degassed, stored in contact with air	30 Jan.		−19	0.66
		60 min, 1 l/min	−19	1.35
	31 Jan.		−17	0.96
	2 Feb.		−15	0.85
W_6 dist. on 28 Jan., treated as W_5	30 Jan.		−16	0.58
		60 min, 1 l/min	−20	1.2
	31 Jan.		−13	0.82
	2 Febr.		−14	0.75
W_7 dist. on 30 Jan., measured some hours later	30 Jan.		−40	0.60
		60 min, 1 l/min	−26	1.15
	31 Jan.		−12	0.70
	2 Feb.		−13	

density, that air-saturated water should have a refractive index that is about $1 \cdot 10^{-6}$ lower than that for air-free water at a temperature of 5–10°C. At higher temperatures, less air is dissolved in the water and the effect should be less. Kirshenbaum also reports (pp. 276 and 295) that the density diminishes when the water is air-saturated. The present author's results obtained with the distilled water agree with those of Tilton and Taylor but not with Kirshenbaum's statement.

From Table 3, one can see that most of the water samples distilled in contact with air gave an increase in refractive index when air was bubbled through them. This is contrary to our earlier findings and thus agrees with Kirshenbaum's statement. The changes in the resistivity indicate, however, that carbon dioxide or some other gas, which is dissociated in the water, is removed. The removal of this gas and the simultaneous saturation with air are two processes that can give an increase in the refractive index. This can also explain the finding reported by Kirshenbaum. Since all of the changes reported are less than 10^{-6} in refractive index and since the instruments used before did not have the high sensitivity of the phase contrast refractometer, too much weight should not be attached to this comparison. The

Table 4. Concentration of the standard heavy water samples used for dilution.

Sample	Concentration weight per cent
I	89.88 ± 0.02
II	95.87 ± 0.02
III	38.48 ± 0.02
IV	94.99 ± 0.02
V	99.13 ± 0.02

purpose of the examination of the water was not to compare with earlier results but to find a standard procedure for the handling of it.

All water used was therefore distilled as described in section 8.1 and then saturated by bubbling with air (90 min with 1 l/min for 2 l water in a 3 l bottle and shorter times for smaller volumes).

9. The heavy water and the measurements performed on it

9.1 *Preparation of the samples*

The concentrated heavy water from which the samples were made by dilution was distilled and treated with air in the same way as the reference water. This procedure can change the D_2O concentration but the present investigation was not concerned with the analysis of the water. The samples were sent to the Swedish Atomic Energy Company for analysis by pycnometer measurements. Five samples of concentrated heavy water were analysed, Table 4. The value used for the specific gravity was $S^{25}_{25} = 1.10775$. The accuracy, ± 0.02 weight per cent in the concentration, given by the Swedish Atomic Energy Company, includes statistical and systematic errors. Due to the treatment of the samples by bubbling air through them, a systematic error may be introduced since air-free water and air-saturated water do not have the same density. According to Kirshenbaum (p. 276), the degassing effect has been reported to influence the density by 0.6 ppm–0.4 ppm. This corresponds to an error in the analysis of less than 0.001 mol per cent and can thus be neglected since it is smaller than the limits in Table 4.

About 60 cm³ of each sample was prepared. For the less concentrated samples, this was done in two steps in order to minimize the influence of the balance and its weights. The weighings are differences of two readings and the maximum error is thus about 0.2 mg. Since the weights of the liquids were always several grams, this gives an error which, even for the lowest concentrations, is less than 0.001 mol per cent. All weighings were corrected for bouyancy. The barometric pressure, the relative humidity and the temperature were determined to better than 0.2 mm Hg, 5 % and 0.2°C (the temperature of the room could vary by such a large amount because the thermostating device had too low a capacity). The relative influence of these errors on the density of the air is 10^{-4}. The effect on the concentrations due to errors in the bouyancy correction is less than that from the other errors.

All handling of the heavy water during the dilutions was made in dry boxes with a thoroughly washed, rinsed and dried syringe so that the dilution of the water by the moisture in the air was kept to a minimum. The syringe was always wetted with a little of the water to be handled in it before the desired amount was sucked up.

The maximum error in the relative concentrations of the samples within a series due to the weighing errors and other known errors is of the order of 0.001 mol per cent. In a few cases, however, accidental errors during the handling may have introduced larger errors. This is indicated by the spread of the points (cf. Figs. 28 and 29 in section 9.4). Since the series were made using different standard water samples, a systematic difference between them may be obtained (cf. Table 4).

The concentrations of the heavy water samples can be expressed in different ways. According to Luten (24), the refractive index difference relative to ordinary water is a linear function of the mol fraction of heavy water. The present author's measurements show that the deviation from linearity is less when mol fraction is used instead of weight per cent. The concentrations are expressed as mol fraction by using the formula:

$$\frac{y\,M_{D_2O} + z\,M_{H_2O}\,(1 + k_y - k_z)}{y\,M_{D_2O} + z\,M_{H_2O}\,(1 + k_y - k_z) + a\,[(1 - y)\,M_{D_2O} + (1 - z)\,M_{H_2O}\,(1 + k_y - k_z)]}$$

where y = weight fraction of D_2O in the concentrated solution
z = weight fraction of D_2O in ordinary water (=0.00016, see e.g. ref. (28))
M = weights of standard heavy water and ordinary water
k are terms that correct the readings for the bouyancy (k_y for heavy and k_z for ordinary water). a = ratio of molecular weights of heavy and ordinary water.

The formula gives the mol fraction deuterium and not the mol fraction D_2O in the water because, as is well known, there is an equilibrium between D_2O, HDO and H_2O molecules in the water. However, in older publications and in analyses of heavy water solutions, the notations "heavy water" and D_2O are commonly used and the author has preferred to follow this terminology.

The factor a was calculated from the known values of the atomic constants determined by mass spectroscopy and compiled by several authors (34) and from the isotopic composition of heavy and ordinary water. The O^{18}/O^{16} ratio for ordinary water has been determined in several laboratories and the mean value 1:504, see Kirshenbaum (28), agrees well with the value obtained for tap water in Stockholm by Isberg and Lundberg (35). The previous value 0.0032 for the Norwegian heavy water has been considered a little doubtful. The new value, 0.00224, from two independent mass spectroscopic determinations (35) seems well established. Using these values and taking into account the small amount of O^{17}, we get the factor $a = 1.11174$.

9.2 *Changes in the D_2O in the cell*

The heavy water in the cell is in contact with glass, silver, nickel and paraffin wax. The slight solvation of the glass or metal will give changes in the refractive index of the order discussed in section 8.2. An exchange with the saturated hydrocarbons in the wax was, however, as reported in the previous publication (3), not to be expected. For some of the more concentrated solutions, a change in the refractive index between the last two measurements on the sample was obtained. It corresponded to a lowering of the D_2O concentration. By assuming the same dilution at each change of sample in the cell, a correction could be made. The largest correction was for the most concentrated sample and corresponded to 0.01 mol per cent. This change can be due to exchange in the cell or to dilution by moisture in the dry box since the flask had to be opened several times. The last explanation is the more probable one since, otherwise, the effect would have appeared for more samples and in a regular way.

9.3 *Measurements on the D_2O samples*

The measurments on the heavy water were made in five series, two at a temperature of 21.65°C and three at 20.03°C, in order to determine the influence of temperature on $n_{D_2O} - n_{H_2O}$. The samples were measured as described in section 7.3. The first readings were taken each day using reference water in both chambers in the cell. The standard water, which was used for the dilutions, was then measured against the reference water. Each heavy water sample was thereafter measured in the same way and the part of the refractive index difference relative to the standard water which corresponded to the fraction of an interference period was then calculated. In order to detect variations in the reference water in the cell during the day, both standard water and reference water were filled into the sample cell after the measurements on the heavy water samples were finished and their readings then determined. The values obtained showed that there had often occurred, during the day, a change in the standard water in its flask and in the reference water in the cell of up to $5 \cdot 10^{-8}$ in refractive index. (Values for some representative series are published in (36).) Since the changes were of such a small magnitude, they could be neglected.

The results of the different series are collected in Table 5 where the numbering of the series corresponds to the dilution of the water samples I–V in Table 4. The concentration values calculated from the formula in section 9.1 give the absolute D_2O concentrations and are corrected for the D_2O content in ordinary water, viz. 0.0148 mol per cent. The values for the refractive index differences were obtained from the fraction of an interference period, measured as above, and a number of whole periods which was calculated from the expected value for the refractive index differences for the respective concentrations. The first measurements were made on low heavy water concentrations and the relation $\Delta n/x$, calculated for each measured sample, was then used in a continuous extrapolation so that this relation described a smooth curve. This gave only one possible value for the number of whole interference periods. Since O^{18} and O^{16} have different refractive indices, the Δn-values are corrected for the enrichment of O^{18} using a formula similar to the one for D_2O together with the relation, $\Delta n = +8 \times c \times 10^{-4}$, determined by Lewis and Luten (23), where c is the O^{18} excess in the samples. Even though this formula is not very accurate, the errors from it are negligible since the corrections are small, viz. $20 \cdot 10^{-8}$, even for the most concentrated solutions. The corrections are, however, applied in order to avoid a systematic error.

From Table 5 and Figs. 28 and 29 where $\Delta n/x$ is plotted as function of the concentration x, it can be seen that the relation between Δn and x is not linear. The value decreases with increasing x. It can also be seen in the figures that there is a spreading of the points. Since all concentrations are assumed to be exact, all of the deviations will appear in the refractive index values. The maximum error 0.001 mol per cent within a series corresponds to 5 in the last figure of the Δn-value. When taken to-

Table 5. The refractive index differences $\Delta n = n_{D_2O} - n_{H_2O}$.

Excess mol per cent D_20	$\lambda = 5461$ A		$\lambda = 4358$ A	
	$-\Delta n \times 10^8$	$\frac{-\Delta n}{x} 10^6$	$-\Delta n \times 10^8$	$\frac{-\Delta n}{x} 10^6$
Series I $t = 21.65°C$				
0.855	4 122	4 822.7	4 486	5 248.6
1.758	8 505	4 837.6		
3.609	17 423	4 827.5	18 966	5 255.0
4.521	21 845	4 831.7		
6.305	30 548	4 831.1	33 156	5 259.0
18.714	90 312	4 825.8		
8.677	41 878	4 826.3	45 569	5 251.7
10.478	50 580	4 827.3	55 062	5 255.0
12.433	60 005	4 826.4		
13.765			72 335	5 254.8
17.878	86 272	4 825.5		
23.002	110 981	4 824.8		
Series II $t = 21.65°C$				
0.899	4 336	4 823.1		
1.692	8 164	4 823.9	8 884	5 249.4
2.832	13 658	4 823.1	14 861	5 247.9
5.592	26 982	4 824.9	29 359	5 250.0
16.133	77 789	4 821.8	84 686	5 249.3
11.215	54 081	4 822.4		
19.884	95 875	4 821.7	104 392	5 250.1
28.661	138 145	4 820.0	150 393	5 247.4
31.742	152 986	4 819.7	166 546	5 246.9
0.841	4 056	4 821.1	4 417	5 250.2
7.170	34 573	4 821.9		
18.778	90 536	4 821.3	98 582	5 249.8
20.914	100 831	4 821.2	109 769	5 248.5
26.170	126 159	4 820.8	137 337	5 247.9
34.822	167 839	4 919.9	182 697	5 246.6
Series III $t = 20.03°C$				
1.002	4 877	4 867.3	5 309	5 298.4
2.710	13 188	4 866.2		
5.403	26 298	4 867.3	28 623	5 297.6
7.286	35 471	4 868.2	38 598	5 297.4
11.384	55 401	4 866.7	60 295	5 296.6
35.990	175 061	4 864.1	190 492	5 292.9
9.350	45 511	4 867.6	49 525	5 296.9
13.399	65 215	4 867.2	70 969	5 296.7
16.972	82 603	4 867.0	89 890	5 296.4
20.814	101 281	4 866.3	110 216	5 295.4
25.105	122 149	4 865.5	132 927	5 294.8
3.150	15 335	4 868.4	16 688	5 297.9
6.228	30 327	4 869.5	32 998	5 298.4
15.214	74 042	4 866.7	80 578	5 296.3
19.006	92 496	4 866.6	100 650	5 295.6
29.851	145 220	4 864.9	150 028	5 293.9

Table 5 (ctd.)

Excess mol per cent D_2O	$\lambda = 5461$ A		$\lambda = 4358$ A	
	$-\Delta n \times 10^8$	$\frac{-\Delta n}{x} 10^6$	$-\Delta n \times 10^8$	$\frac{-\Delta n}{x} 10^6$
		Series IV $t = 20.03$°C		
2.071	10 083	4 867.7	10 967	5 294.5
4.239	20 624	4 865.2	22 446	5 295.2
34.419	167 285	4 860.2	182 041	5 288.9
6.361	30 940	4 864.3	33 670	5 293.5
10.169	49 451	4 862.9		
20.121	97 825	4 861.7	106 458	5 290.8
		Series V $t = 20.03$°C		
4.786	23 293	4 867.4	25 342	5 295.6
9.483	46 120	4 863.4	50 212	5 294.9
13.972	67 966	4 864.5	73 973	5 294.4
18.803	91 459	4 864.1	99 534	5 293.6
27.034	131 490	4 863.9	143 078	5 292.5
25.256	122 844	4 863.9	133 679	5 292.9
38.664	187 998	4 862.3	204 555	5 290.5
56.862	276 334	4 859.8		
74.754	363 121	4 857.6	395 065	5 284.9
99.019	480 587	4 853.5	522 839	5 280.2
26.058	126 739	4 863.8	137 926	5 293.1
43.205	210 070	4 862.2	228 584	5 290.7
63.024	306 235	4 859.1	333 201	5 286.9
83.775	406 812	4 856.0	442 599	5 283.2

gether with the deviation in the measurement, this gives about 10 in the final figure. The relatively large spread in the $\Delta n / x$-values, Figs. 28 and 29, for low concentrations is due to this error. The spread within series I is larger than that for the other series (cf. the ε-values in Table 6). This is explained by the fact that the technique for measuring and handling the samples was worked out in the first series. The systematic difference between the different series is due partly to the treatment and handling of the samples before and after the analysis and partly to the error in the analysed value (cf. Table 4).

The missing values for one of the wave lengths at various places in Table 5 result from the fact that the value has fallen on or near the maximum or minimum of the calibration curve.

9.4 *The equations for* $n_{D_2O} - n_{H_2O}$

Equations can be fitted to the values in Table 5. The combination of the $(n - 1)$ (Dale-Gladstone) or $(n^2 - 1)/(n^2 + 2)$ (Lorenz-Lorentz) values for the two components according to Partington (32) indicates that the equations should be of the second or the third degree. The higher terms, however, should be small.

The calculations were made in the usual way by choosing an approximate equation of the second degree for both wave lengths at the two temperatures and then making a closer fit to a 2nd or 3rd degree equation using the method of least squares, see

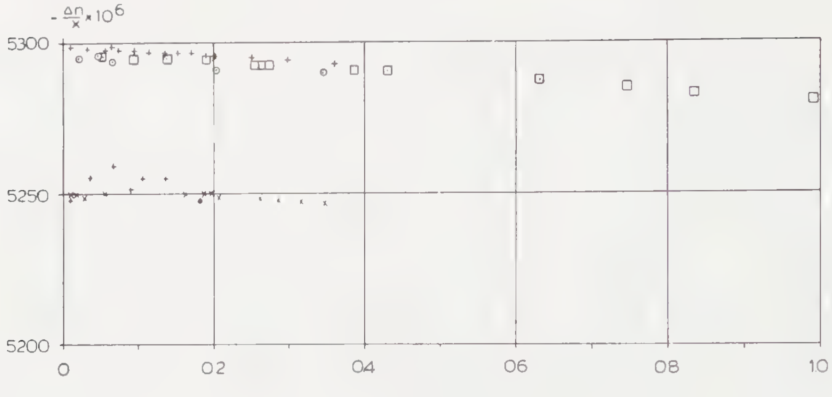

Fig. 28. The value of $-\Delta n/x$ as a function of the D_2O-concentration x. $\lambda = 4358$ A. The points in the upper group are for 20.03 C, viz. series III + + +, IV ○ ○ and V □ □, and in the lower group for 21.65 °C, viz. series I + + + and series II × × ×.

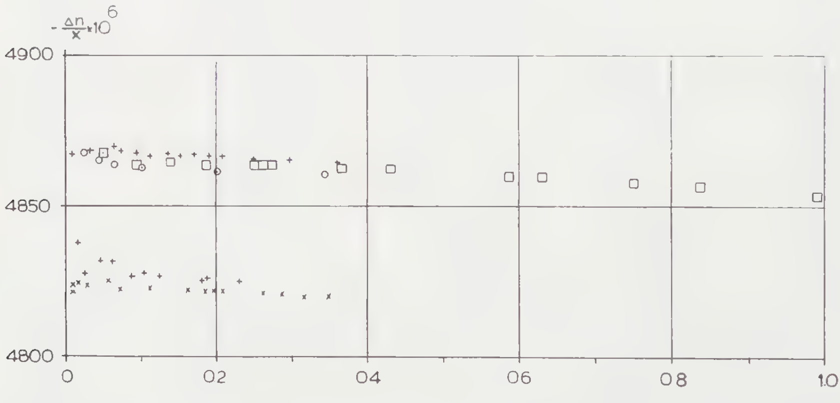

Fig. 29. The value $-\Delta n/x$ as a function of the D_2O-concentration x. $\lambda = 5461$ A. The points are marked for the different series in the two temperature groups as in Fig. 28.

e.g. Whittaker and Robinson (37). However, this can be done in different ways. Taking the three series for $\lambda = 5461$ A and $t = 20.03$ C, it can be seen that there are systematic differences, Fig. 29, and that two of the series stop at about 35 mol per cent. If all values from these series are used in determining one equation, then the values of the series must be given unequal weights. The systematic errors in them would otherwise be given weights proportional to the number of terms in the series and that would not lead to a correct result. If all values are used for one equation, then the values from the shorter series may, due to the systematic errors, especially influence the higher terms, which are mainly determined from the long series, in a manner that would depend on the weights chosen. The weights have to be determined from the spread in the values, the number of terms and the relative accuracy for the different series, cf. Table 4. It was therefore decided to calculate an equation for each series. In the determination of the higher degree terms of the final equation, the values from the long series must be given a much larger weight than those from the short series since the values obtained from the short series are determined to give the best fit up to 35 mol per cent and since the extrapolation to 100 per cent thus can give appreciable errors. In fact, the standard deviations (s.d.) for the higher terms in these short series turned out to be of the same magnitude as the terms themselves due to the spread of the points and the small deviation from linearity. It was thus decided to determine the higher terms from the long series and then fit the shorter ones to equations with different first degree terms. The mean values of the first coefficient for the four equations representing two wave lengths at two temperatures were then calculated. In these calculations, the method of determinants was employed since the values of the cofactors were also necessary for the determination of the standard deviations in the coefficients. The standard deviation ε in a value is obtained from $\varepsilon^2 = \frac{\Sigma (y_0 - y)^2}{s - m}$ where y_0 is the measured value in Table 5, y the value from the equation, s the number of values and m the number of unknown coefficients in the equation (in this case $m = 2$ or 3). The standard deviations in the coefficients are determined from the relations $\varepsilon(x) = \varepsilon \sqrt{\frac{A_{11}}{D}}$, $\varepsilon(x^2) = \varepsilon \sqrt{\frac{A_{22}}{D}}$ ... where A_{11} ... are the minors and D the determinant.

Equations of the second and the third degree have been fitted, in the manner described, to the values in Table 5. The closeness of fit can be estimated from the ε-values. A comparison between them showed that the ε-values for the second and the third degree equations were of the same magnitude (36), most of them being of the order of $10 \cdot 10^{-8}$ in refractive index, cf. Table 6. From the mathematical point of view, either equation could be chosen and the second degree one should therefore be preferred. A calculation of the equation from a theoretical formula (32), using the latest data for the different values in it, showed that the third degree term should be negligibly small, cf. below, and this also showed that the simpler second degree equations should be chosen. The equations for the different series are shown in Table 6. By comparing the last two columns, the approximation made by using, for the short series, the coefficient for x^2 from the long series can be seen. The increase in ε is not great. The photometric sensitivity corresponds to an error of 3 units in the determination and the calibration curve can give an error of 5 units so the equations fit rather well to the experimentally determined points.

From the equations in Table 6 for the series and from the points in Figs. 28 and 29, it can be seen that there are systematic differences between the series of the same relative magnitude as the accuracy given in Table 4 for the analyses. Of course, this difference is not only dependent on the analysis method but also on the subsequent handling of the water because systematic errors can have been introduced during the dilution procedure. During the purification of the water, errors may have been introduced which influenced the gravimetric and refractometric methods in opposite directions. Hence, these possible effects could also be partly responsible for the difference. However, in the calculation of the mean equation, different weights should be given to the series. Series III is given the weight $\frac{1}{2}$ and the others the weight 1 (cf. Table 4). For 20.03°C, we thus get the equations

Table 6. Equations for $y = f(x)$.

		ε	ε for the best fit
	$\lambda = 5461$ A		
Ser. V	$y = 486\,787\,x - 1427\,x^2$ s.d. 31 s.d. 40		18
Ser. IV	$y = 486\,502\,x - \cdots$	7	6
Ser. III	$y = 486\,913\,x - \cdots$	5	5
Ser. II	$y = 482\,434\,x - \cdots$	8	7
Ser. I	$y = 482\,849\,x - \cdots$	12	11
	$\lambda = 4358$ A		
Ser. V	$y = 529\,760\,x - 1735\,y$ s.d. 67 s.d. 81		19
Ser. IV	$y = 529\,477\,x - \cdots$	6	6
Ser. III	$y = 529\,898\,x - \cdots$	4	3
Ser. II	$y = 525\,253\,x - \cdots$	9	9
Ser. I	$y = 525\,660\,x - \cdots$	20	19

$$\lambda = 5461 \text{ A} \quad -\Delta n \times 10^8 = 486\,698\,x - 1427\,x^2 \qquad [7]$$

$$\lambda = 4358 \text{ A} \quad -\Delta n \times 10^8 = 529\,674\,x - 1735\,x^2 \qquad [8]$$

In order to see how well the calculated equation describes the non-linearity of the Δn-function, the differences between calculated and measured values, used in the calculation of ε, can be compared for example for series V using the equation in Table 6 and the values in Table 5, thus excluding systematic errors. The deviations for the higher concentration were not larger than those for the low ones, cf. (36). This showed that the equations describe correctly the non-linearity and hence that the use of the equations in the analysis procedure is justified. The deviations for blue light were found to be greater than those for green. The previously given photometric accuracy is for green light. The blue light had a much lower intensity but this was partially compensated for by the higher spectral sensitivity of the photocell for blue light. Only one phase plate was used for this wave length instead of the two for the green light. This also means that the values obtained with green light are more accurate since most of them are a mean for both plates. Indications were also obtained that, in a few cases, the samples could have been influenced in some unknown way during the measuring procedure since the deviations for both wave lengths had the same sign and magnitude, viz. up to 30×10^{-8} in refractive index.

The standard deviation in the coefficient for x^2 can be put equal to the value in Table 6. The error in the coefficient for x depends on the accuracy and spread in the coefficients for the different series. The spread within each series is about the same, judging by the ε-values in Table 6 and the spread in the points of Figs. 28 and 29. The values for series V can be chosen as representative for this influence. Since the number of series in the two temperature groups is small, viz. two in one and three in the other, it is not strictly correct to calculate a standard deviation for the mean value of the x coefficient. Nevertheless, the author has chosen to use Gauss' error theory since these standard deviations are to be combined with the standard deviations within a single series. The standard deviations for the mean values are calculated with the same weights as above. The values 118 and 119 were obtained for the respective wave lengths. Combining by means of the square root law, we get the values 122 and 137 respectively.

From the series for the two temperatures, the temperature derivative for $n_{D_2O} - n_{H_2O}$ can be obtained. Since the same x^2 coefficient is assumed for all series, the influence of the temperature is completely contained in the first term. An influence from the second degree term, giving a non-linear temperature derivative with respect to the concentration, may exist but cannot be determined from the present material since, for one of the temperatures, the series were only given up to 35 mol per cent. From the mean values for the two groups, the temperature derivative was determined. Using the standard deviations for the equations giving these values together with the error in the temperature determination, which was at most 1 %, the standard deviation was found to be 6.0 per cent or, in absolute units, 1.5×10^{-6} and 1.6×10^{-6} respectively for the two wave lengths.

From the equations for 20.03°C and the temperature derivatives, the equations for 20.00°C can be calculated. Since the difference in temperature is small, no errors resulting from the derivatives will be introduced. The following relations were obtained for $\Delta n = n_{D_2O} - n_{H_2O}$ (x = excess D_2O concentration). All n-values are relative to air at 20°C and 760 mm Hg—this temperature was chosen instead of 15°C which corresponds to the definition of "standard air", since 20°C is closer to the temperature of modern laboratories, cf. section 7.2.1.

$\lambda = 5\,461$

$$-\Delta n \times 10^7 = 48\,662 \text{ (s.d. } 12) x - 143 \text{ (s.d. } 4) x^2 \qquad [9]$$

$$\frac{d(\Delta n)}{dt} \times 10^6 = 25.0 \text{ (s.d. } 1.5) x \qquad [10]$$

$\lambda = 4\,358$ A

$$-\Delta n \times 10^7 = 52\,960 \text{ (s.d. } 14) x - 174 \text{ (s.d. } 8) x^2 \qquad [11]$$

$$\frac{d(\Delta n)}{dt} \times 10^6 = 26.0 \text{ (s.d. } 1.6) x \qquad [12]$$

In the standard deviation for the first term, all influences on the determinations have been included, viz. from the purification and handling of the concentrated heavy water, the analysis, the dilution and the refractometric measurements etc. The thermometer used for the determination of the true temperature was calibrated by the Swedish National Institute for Material Testing. According to the National Institute, it was compared with a secondary standard which had a maximum error of 0.01°C and the readings were made by estimating the fraction of a scale division to 0.01°C. The maximum deviation from this calibration, which is not included in the equations, is thus of the order of 5 units in the x-coefficient in equ. [9] and [11]. The relative error from the cell thickness, section 7.2.1, is 5×10^{-5} which will slightly increase the standard deviation given for the first coefficient.

The equations [9] and [11] can be compared with each other and with theoretical equations obtained by combining the components in the mixture and their n-values.

According to Partington (32) p. 72 etc., the combining of these values can be made in different ways. It has been found that many solutions follow the simple law $v(n-1) = \Sigma v_i(n_i - 1)$ where v and n are the volume and refractive index for the solution and v_i and n_i those for the components in it. This formula has been used in the present paper. In the calculation, it is necessary to know the relation between the density of the solution and the mol fraction deuterium in it since the volumes are obtained from the masses and densities. The relation can be obtained from (24) but, since these values are rather old, the relation in (28), calculated with the assumption of additive molar volume relationships, was used. The refractive index difference $n_{H_2O} - n_{sample}$ was obtained as the product of the difference $n_{H_2O} - n_{D_2O}$ multiplied by a polynomial. In calculating the coefficients in it, the factor a, section 9.1, and the specific density at 20°C were used. The coefficients converge very rapidly, the third degree term gives, even for pure heavy water, a contribution of less then 10^{-7} in n so all terms except the first and second can be neglected. The second degree terms in these calculations were found to be 191 and 208 respectively when the theoretical equations were determined to give the same Δn-values for $x = 1$ as the experimental ones. The difference between the theoretical and experimental equation are thus for $\lambda = 5461$ A $-\delta n \times 10^7 = 50x - 49x^2$ and for $\lambda = 4358$ A $-\delta n \times 10^7 = 35x - 35x^2$. The maximum difference, at x about 0.5, is of the order of 10^{-6} in refractive index. This value would have been lower if the best fit between the equations had been made, i.e. they shall not coincide at $x = 1$ (36). In the determination of the theoretical equation only the two components D_2O and H_2O were assumed (the same is valid for Kirshenbaum's calculation of the density-mol fraction relation).

There is an equilibrium between D_2O, HDO and H_2O molecules in the solution, at low and high concentrations there is almost no D_2O or H_2O in the water. This ought to have been considered in the theoretical calculation. However, no values for the density and refractive index of HDO are available so it could not be done. The calculated second degree terms are, for both wave lengths, larger than the experimental ones, so taking account of HDO might have given a still better agreement. However, since the difference between the equations for each wave length is small, the refractive index of the solution is accurately described by the simple law used above. The use of $(n^2-1)/(n^2+2)$, which is a more theoretical expression for the refractivity, instead of $(n-1)$ gives a more complicated calculation for Δn and was therefore not used since the simpler relation gave a good agreement. (A calculation using the relation from (24) for the density gave large second and third degree terms and a poor fit with the experimental equation.)

The dispersion can be obtained by comparing equations [9] and [11]. According to the theory above, the terms in equation [11] should be 10 % higher than in equation [9]. The second degree terms differ a little more but the boundary limits for the values given by the standard deviations indicate that a difference larger than 10 % is perhaps not real. Further examinations in the high concentration region may decide this question.

The temperature derivatives, formulae [10] and [12], are linear with respect to concentration since the same second degree term was assumed in the calculations of all equations for each of the two wave lengths. A non-linearity may exist but cannot be obtained from the present material. By using a larger temperature difference, it may be possible to find whether there is a non-linearity. Since the n-value is larger for blue light than for green, it is reasonable to suppose that the temperature derivatives are in the same proportion.

9.5 *Comparison with earlier determinations, analytical possibilities*

For pure heavy water with no O^{18} enrichment, the present author's formulae give $n_{H_2O} - n_{D_2O} = 0.004852$ and 0.005279 for $\lambda = 5461$ and 4358 Å respectively. A comparison with earlier determinations may be made preferably with Stokland's values (27) since they were determined on concentrated heavy water after its specific density had become well established. His results are 0.004832 and 0.005272. The data given in the paper concerning the experimental technique are rather meagre so it is difficult to discuss the reasons for this discrepancy. According to the previous section, the present author's values have a maximum error of 2 in the last figure if the systematic errors are also included. The difference cannot be due to the same reason for both wave lengths since the value for $\lambda = 4358$ Å does not differ as much as the other. The influence of O^{18} enrichment is smaller than this difference provided that the enrichment has not changed since Stokland's determinations. If the water had at that time contained 0.0032 % O^{18}, then 0.000010 should be added to his values and this would give a better agreement with the values obtained here.

Our previous values (3) are, as mentioned before, not reliable since the examination of the water, the calibration curve of the instrument and other factors were not kept under sufficient control at that time. The concentrations measured were, in addition, rather few. A comparison with those results is therefore of little significance.

The value of the temperature derivative can be compared with the determination of Filippova and Slutskaya (38). They give for heavy water the value, $+24.0 \times 10^{-6}$ for the wavelength 5876 Å. This value is lower than those obtained here but the present work indicates that the temperature derivative decreases with an increase in wave length so the actual difference may not be so large. Their value is valid in the temperature interval 18–25 °C which includes the temperature at which the present measurements were made. The limits for the errors in their determination were not given and cannot, moreover, be deduced from the publication.

The phase contrast refractometer seems to give an alternative method for the analysis of heavy water samples. The accuracy that can be obtained depends on the concentration. In the concentration region from zero up to a few per cent, the accuracy will in this case be determined, since the error in the coefficients is of smaller influence, by the reproducibility of the handling of the water samples and by the photometric accuracy in the determination of the intensity ratio in the image. These two factors combined together give as maximum error about 15×10^{-8} in refractive index difference (cf. section 8) which corresponds to 0.002 mol per cent. In the higher concentration regions, the maximum error increases continuously and, for the most concentrated water samples, it is about 0.02 mol per cent. A higher accuracy can be obtained if refractive index determinations are made on a larger number of samples so that the coefficients in equ. [9] and [11] are obtained with lower standard deviations.

If only a small range, e.g. 0–0.5 % or 99–100 %, is to be used for analysis, it is then more suitable to calibrate the instrument using known concentrations. Many of the factors discussed above which are responsible for the lowering of the accuracy—in particular those which constitute possible sources for systematic deviations—will then be avoided. This procedure also automatically compensates for the influence on the refractive index from both the enrichment of O^{18} and the content of D_2O in the

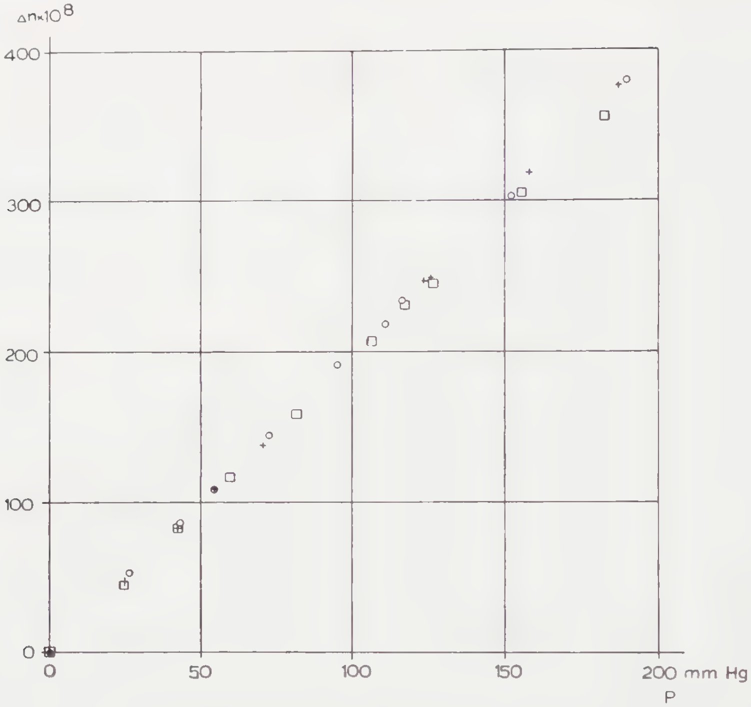

Fig. 30. The change of refractive index with compression for ordinary water. Points marked in the same way belong to the same series.

ordinary water used as reference in the measurements. Used in this way, the phase contrast refractometer will give the same accuracy as that for the standard solutions determined by gravimetric methods.

10. Determination of the compressibility coefficient

As mentioned briefly before, it is necessary to make certain, when using an instrument with such a high sensitivity as that of the phase contrast refractometer, that the influence of the compression on the refractive index of the liquid is under control. Many relations describing $n = f(\varrho)$ have been given, see e.g. Partington (32), and they have, in various cases, given good agreement with experimental values. In order to test Dale-Gladstone's formula, which has proved to be good for liquids, the influence of the compression on the refractive index of heavy and ordinary water has been measured here. The compressibility coefficients were then calculated and compared with values obtained in other investigations.

10.1 *Measuring procedure*

The cell was filled with sample in the usual manner. In order to prevent any change of the liquid in the cell during a series, the inlet tubing, which was of course full of liquid, was closed and the overpressure was applied to the outlet tubing by using

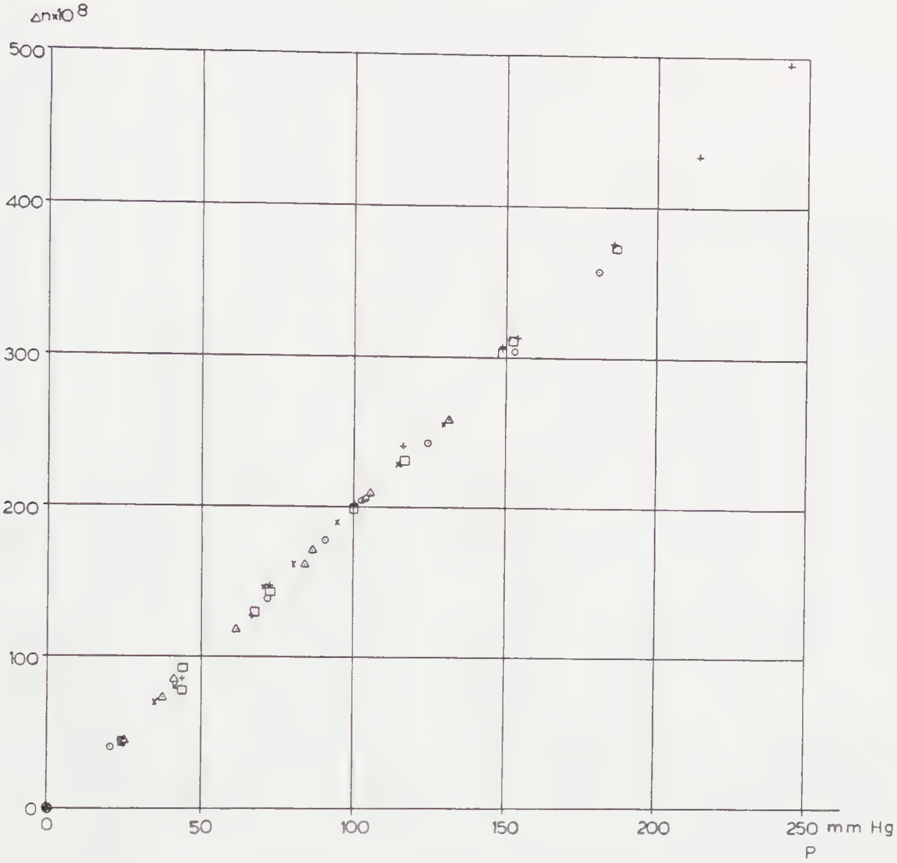

Fig. 31. The same relation as in Fig. 30 for an 80 % heavy water sample. Points marked as in the previous figure.

the gas system in Fig. 25 together with dry, carbon dioxide-free air from a bomb. Since the largest pressure used was about 250 mm Hg, the force on the glass plates in the sample cell was at most about 1.5 N which was too small to produce any change in the cell since the forces from the rubber rings pressing on the surfaces were much larger. The measurements were made on ordinary water and on a sample of heavy water with a concentration of 80 weight per cent at a temperature of 20.0° C. Several series were determined over a period of a few days. The values obtained, Table 7, are shown in Fig. 30 for ordinary water and in Fig. 31 for the heavy water sample. The Δn-values are counted from the n-value for $p = 0$ which, for ordinary water, was near a minimum on the calibration curve, Fig. 26, but which, for the heavy water sample, could occur at any point. For some of the series, it was rather close to a maximum. This zero point was therefore not more accurately determined than the rest of the points.

Table 7. The relation between the pressure and Δn.

a. *Ordinary water.*

Series I		II		III	
p mm Hg	$\Delta n \times 10^8$	p mm Hg	$\Delta n \times 10^8$	p mm Hg	$\Delta n \times 10^8$
24.9	47	26.7	53	23.6	46
42.3	83	43.0	83	42.5	82
70.5	138	72.5	145	81.8	159
99.8	198	94.9	191	105.8	207
125.8	249	116.7	234	125.8	247
157.2	318	152.1	303	155.4	305
187.1	376	189.5	379	182.0	356
123.5	247	110.5	219	117.3	231
54.4	109	54.0	109	59.7	118

b. *Heavy water,* 80 weight per cent.

Series I		II		III		IV		V	
p mm Hg	$\Delta n \times 10^8$	p mm Hg	$\Delta n \times 10^8$	p mm Hg	$\Delta n \times 10^8$	p mm Hg	$\Delta n \times 10^8$	p mm Hg	$\Delta n \times 10^8$
20.5	40	72.6	148	23.7	46	24.7	46	24.1	46
42.5	85	100.4	202	42.3	80	37.3	73	43.2	89
71.6	139	116.6	241	70.8	143	61.5	120	72.6	145
104.0	205	153.7	313	94.6	189	83.9	162	100.4	200
124.1	242	185.9	376	114.6	228	104.9	209	116.6	232
152.3	303	211.3	433	129.4	255	130.6	258	153.7	311
180.2	357	243.7	495	80.8	161	87.1	172	185.9	374
102.0	204	148.3	307	35.4	69	41.1	82	148.3	305
43.4	86	67.6	127					67.6	139
		44.4	86					44.4	93

10.2 *Calculation of the compressibility*

For the calculation of the compressibility coefficient $\varkappa$ from the formula $n = f(p)$, the quotient $\Delta n / \Delta p$ is required. From the points in Figs. 30 and 31, it is seen that the relation between Δn and the pressure is linear in the region measured. This region corresponds to only small overpressures. Using the method of least squares, all points for the samples can be used to determine a single equation. The standard deviations of its constants can then be obtained as before. However, the series measured were determined on different days and contain, moreover, a different number of points which means that they should be given different weights. It was decided to calculate, instead, the constants in the equation for each series and then take the mean of them. The standard deviation was, as before, used as a measure of the spread although the number of series was small. The point $p = 0$ had the same weight as the rest of the points and it was therefore not certain that the straight line would pass through the origin. The equation $n = a + bp$ was thus chosen.

For ordinary water, the following values for $b = \Delta n / \Delta p$ were obtained (in $\Delta n \times 10^6$/m Hg):

20.19 (s.d. 0.10), 20.01 (s.d. 0.08) and 19.62 (s.d. 0.05)
and for 80 % heavy water:

19.81 (s.d. 0.11), 20.45 (s.d. 0.18), 19.94 (s.d. 0.16), 19.83 (s.d. 0.15) and 20.20 (s.d. 0.16).

From Dale-Gladstone's formula, $n - 1 = k\varrho$, we get $\frac{\Delta n}{n-1} = \frac{\Delta \varrho}{\varrho} = \varkappa \Delta p$. Inserting the values for the density of mercury at 20°C and for $(n-1)$, the relations $\varkappa = \frac{\Delta n}{\Delta p} \times 2.2538 \times 10^{-5}$ m²/N for ordinary water and $\varkappa = \frac{\Delta n}{\Delta p} \times 2.2812 \times 10^{-5}$ m²/N for the 80 % heavy water are obtained. This gives $\varkappa = 44.9$ (s.d. 0.4) $\times 10^{-11}$ m²/N and $\varkappa = 45.7$ (s.d. 0.4) $\times 10^{-11}$ m²/N respectively. The standard deviations given include the standard deviation for each series and for their mean value. If a linear dependence with concentration is assumed, an extrapolation to 100 % heavy water gives $\varkappa = 45.9$ (s.d. 0.4) $\times 10^{-11}$ m²/N. The zero-values for the heavy water series showed that its concentration decreased slightly, by some tenths of a percent, from the first to the last day. This decrease is, however, of no importance since the error from it only influences the small value added in the extrapolation to the figure for the 80 % sample. It is in fact not necessary to know the concentration to better than within a few percent.

10.3 *Discussion*

The values given above show rather large relative errors. This is due partly to the fact that the total refractive index differences are small, viz. of the order of 400×10^{-8}. The pressures were determined to 0.2 mm Hg using a cathetometer and the influence of errors in the pressure readings was also incorporated in the standard deviations given above. The standard deviations were the same for ordinary and heavy water, thus indicating that no effects due to dilution had effected the heavy water results. For the heavy water, the measurements were made on the slope of a period with an interference order of about 215. In section 5, it was shown that the contrast had not changed for these orders of interference so the contrast was the same as that for the first periods. The Δn-values determined from the drum readings and the calibration curve had therefore no systematic errors of this kind.

The values determined in this way may be compared with those published by Kirshenbaum (28). For the isothermal case, he gives (temp = 25°C) for D_2O 46.4 $\times 10^{-11}$ m²/N and for H_2O 45.0 $\times 10^{-11}$ m²/N. These values were determined from the velocity of sound in water. For ordinary water, the agreement is good but, for heavy water, the value obtained in this work is lower. Although the present author's values are not so accurate, they indicate that heavy water has a higher compressibility than ordinary water. This agrees with Kirshenbaum's values. There are, however, other values published which indicate the contrary but these are, according to Kirshenbaum, not so reliable.

This comparison indicates that the law, assumed by Dale-Gladstone for the relation between density and refractive index, in fact describes this relation accurately since the values calculated using it agree well with those obtained by other methods.

Other functions, e.g. Lorenz-Lorentz, were found to be less satisfactory. The Dale-Gladstone refractivity was also used in the author's calculations of the function, $n_{D_2O} - n_{H_2O} = f(x)$.

ACKNOWLEDGEMENTS

The author would like to express his sincere gratitude to the head of the Institute of Optical Research, Professor Erik Ingelstam, for valuable discussions during this work. Thanks are also due to Mr. Lars Sjöfall for help with some of the instrument details. The author is indebted to Professor Manne Siegbahn at the Nobel Institute of Physics for supplying the grating, to Dr. Gösta Siljeholm of the Lumalampan Aktiebolag for his construction of the special mercury lamp and to the Swedish Atomic Energy Company for supplying and analysing the heavy water.

Institute of Optical Research and Department of Physics II, Royal Institute of Technology, Stockholm 70. October 1959.

REFERENCES

1. E. Ingelstam, Arkiv för fysik *6*, Nr 29, 1953.
2. E. Djurle, Appl. Sci. Research B *4*, 91, 1954.
3. E. Ingelstam, E. Djurle and L. Johansson, J. Opt. Soc. Am. *44*, 472, 1954.
4. E. Djurle, Arkiv för fysik *11*, Nr 5, 105, 1957.
5. E. Djurle, J. Opt. Soc. Am. *46*, 373 (TD75), 1956.
6. W. S. Rodney and E. Djurle, J. Opt. Soc. Am. *48*, 388, 1958.
7. A. H. Bennet, H. Osterberg, H. Jupnik and O. W. Richards, Phase Microscopy, Principles and Application, John Wiley et Sons, Inc. New York 1951.
8. U. Schmidt, Annalen der Physik (6) *16*, 68, 1955.
9. H. Wolter, Annalen der Physik (6) *7*, 33, 1950.
10. H. Wolter, Encyclopedia of Physics *24*, 555. Springer Verlag, Berlin 1956.
11. P. M. Duffieux, L'Intégral de Fourier et ses applications à l'optique. Rennes 1946.
12. F. Zernike, Physica, *9*, 686 and 974, 1942.
13. R. Barer, Journ. Roy. Micr. Soc. *72*, 10 and 81, 1952.
14. A. A. Michelson, Phil.Mag. *31*, 338, 1891 and *34*, 280, 1892.
15. E. Ingelstam, Optica Acta *2*, 73, 1954.
16. J. Ericsson and L. (Johansson) Sjöfall, Optica Acta, in print.
17. C. Candler, Modern Interferometers, Hilger and Watts Ltd, London 1951.
18. H. Margenau and W. W. Watson, Revs. Modern Phys. *8*, 22, 1936.
19. H. Barrell and J. E. Sears, Phil. Trans. Roy. Soc. A *238*, 1, 1939.
20. B. Edlén, J. Opt. Soc. Am. *43*, 339, 1953.
21. L. W. Tilton, J. Res. Natl. Bureau of Stand. *14*, 393, 1935.
22. R. H. Crist, G. M. Murphy and H. C. Urey, J. Am. Chem. Soc. *55*, 5060, 1933.
23. G. N. Lewis and D. B. Luten, J. Am. Chem. Soc. *55*, 5061, 1933.
24. D. B. Luten, Phys. Rev. *45*, 161, 1934.
25. N. F. Hall and T. O. Jones, J. Am. Chem. Soc. *58*, 1915, 1936.
26. L. W. Tilton and J. K. Taylor, J. Res. Natl. Bureau of Stand. *13*, 207, 1934.
27. K. Stokland, Kgl. Norske Videnskab. Selskabs Forh. *10*, No. 39, 145, 1938.
28. I. Kirshenbaum, Physical Properties and Analysis of Heavy Water, McGraw-Hill Book Company, New York 1951.
29. S. Namba, Rev. Sci. Instr. *27*, 872, 1956.
30. R. Penndorf, J. Opt. Soc. Am. *47*, 175, 1957.
31. Landolt-Börnstein, Physikalisch-Chemische Tabellen Eg IIIb, 1715, Verlag von Julius Springer, Berlin 1935.
32. J. R. Partington, An Advanced Treatise on Physical Chemistry, Vol. IV Physico-Chemical Optics, Longmans, Green and Co., London 1953.
33. L. W. Tilton and J. K. Taylor, J. Res. Natl. Bureau of Stand. *20*, 419, 1938.

34. See, for example, E. SEGRÉ, Experimental Nuclear Physics, Vol. I, John Wiley and Sons, New York 1953 or I. KAPLAN, Nuclear Physics, Addison-Wesley Publishing Co. Reading, Mass. 1956.
35. P. ISBERG and L. LUNDBERG, Zeitschrift f. Naturforschung *9a*, 472, 1954.
36. E. DJURLE, Report 11.11.59, Institute of Optical Research, Stockholm 70.
37. E. WHITTAKER and G. ROBINSON, The Calculus of Observations, Blackie and Son Ltd, London 1958.
38. N. S. FILIPPOVA and M. M. SLUTSKAYA, J. Phys. Chem. U.S.S.R. *8*, 486, 1936.

Tryckt den 24 februari 1960

Uppsala 1960. Almqvist & Wiksells Boktryckeri AB